

Quantum vacuum emission in a nonlinear optical medium illuminated by a strong laser pulse

Stefano Finazzi and Iacopo Carusotto

*INO-CNR BEC Center and Dipartimento di Fisica,
Università di Trento, via Sommarive 14, 38123 Povo-Trento, Italy*

(Dated: July 18, 2012)

A strong light pulse propagating in a nonlinear Kerr medium produces a change in the refractive index, which makes light travel at different speeds inside and outside the pulse. By tuning the pulse velocity, an analogue black hole horizon can be obtained in a suitable frequency window. In this paper, we develop a quantum theory of light propagation for this system, including the frequency dispersion of the refractive index of the medium by coupling the electromagnetic field to matter polarization fields. In a configuration with a single black horizon, the spectrum of spontaneously emitted particles presents a few similarities with Hawking radiation. In horizonless system spontaneous vacuum emission is still possible due to the dispersive nature of the medium, yet with different spectral properties.

PACS numbers: 04.62.+v, 42.65.-k

I. INTRODUCTION

Hawking radiation [1, 2] is the quantum production of particles from vacuum fluctuations due to the presence of a black hole horizon in a curved stationary geometry. In the pioneering work [3], it was shown that this prediction does not reside on the peculiar dynamical features of a general-relativistic spacetime, but only on the kinematic properties of a quantum field living in a curved spacetime. As a result, analogous quantum vacuum emission phenomena have been anticipated to occur in several physical systems, ranging from flowing fluids and superfluids, to ion rings, to nonlinear optical systems [4]. In particular, the advanced techniques of pulse manipulation and light detection that have been developed in the recent years put nonlinear optical systems among the most promising candidates for the realization of analogue models of gravitational systems.

In addition to the many proposals that appeared in the last few years [5–8], the first claim of observation of an analogue Hawking radiation in a laboratory was reported in [9, 10] using the refractive index change induced by a strong laser pulse propagating across a nonlinear dielectric medium. The velocity of the pulse can be tuned either by changing the laser wavelength or by using an axicon with different angles to produce a Bessel beam [11–13]). In this way the speed of optical frequency photons inside the pulse can be made smaller than the pulse velocity, while the one outside the pulse remains larger. Consequently, the boundaries of the pulse appear as analogue horizons, as seen from the frame comoving with the pulse. Unfortunately, the observation of Hawking emission in this system is still considered as controversial by some authors, who recently raised a few issues [14, 15]. In spite of attempts of alternative theoretical interpretation [16, 17], no satisfactory explanation of the experimental observations has been found yet.

Differently from previous studies that deeply reside on the analogy with gravitational physics, the present

work develops a microscopical quantum optical model of light propagation in a nonlinear dielectric modulated by the passage of a high-intensity laser pulse. The structure of modes propagating in a one-dimensional system is described by using the Lagrangian of the electromagnetic field coupled with three polarization fields. In this way, we are able to canonically quantize a theory which exactly reproduces the complete Sellmeier dispersion of transparent materials such as the fused silica used in the experiment [9]. This allows us to describe the system in a far more realistic way than existing works based on simplified subluminal dispersions [18, 19] and obtain quantitative predictions for the spectrum of spontaneously emitted photons under the simplifying assumption that the strong pulse propagates through the medium in a steady and rigid way and that the jump in the spatial profile of the refractive index is very sharp.

In particular, we point out how the highly nontrivial dispersion relation makes the analogy with standard quantum field theory in curved spacetime much weaker than in other analogue systems considered in the literature, such as Bose-Einstein condensates [4]: for instance, in the present nonlinear optical context, an analogue horizon can be defined only in a finite frequency range [20] that does not extend to the long-wavelength limit where the analogue geometry is generally defined. Nonetheless, the properties of the quantum vacuum emission in this frequency range share several features of standard Hawking radiation.

Furthermore, in contrast to non-dispersive media, where a necessary and sufficient condition to trigger emission processes *à la* Hawking is the presence of analogue horizons, quantum vacuum radiation occurs in dispersive media even in the absence of any horizon as soon as the dispersion allows for modes with a negative norm (with respect to the natural scalar product induced by the symplectic structure of the Hamiltonian) and a positive frequency as seen from the pulse comoving frame [20]. With respect to the above mentioned Hawking-like emis-

sion channel, this additional emission is generally much weaker.

The structure of the article is the following. In Sec. II, we start from the Lagrangian to derive and solve the equation of motion for the electromagnetic field coupled to matter polarization fields. In Sec. III, the properties of the eigenmodes are investigated in the most significant configuration with a single analogue black hole horizon, and the two bases of in- and out-going scattering modes are built. In Sec. IV, the spectrum of emitted particles is computed in the case of a large refractive index jump between the two sides of the analogue black hole horizon. The more realistic case of a small refractive index jump is studied in Sec. V along with the horizonless configuration recently realized the experiment [9]. Conclusions are finally drawn in Sec. VI.

II. THE GENERAL FRAMEWORK

In this section we develop the quantum theory used to describe light propagation in a dielectric medium with a refractive index modulation that moves in space at a uniform velocity v : in the experiments, the refractive index change is generated by the strong pulse via the Kerr nonlinearity of the medium. At a simplest level of approximation, one can assume that the refractive index change follows locally in space and instantaneously in time the intensity profile of the pump pulse [21].

The optical properties of the medium are described in the spirit of the Hopfield model [22] in terms of an electromagnetic field interacting with a polarization field. To closely reproduce the Sellmeier dispersion relation of typical transparent dielectrics such as fused silica [9], the polarization of the medium has to show three poles with different strengths and frequencies. The effect of the passage of the pulse in the medium is then modeled as a spatio-temporal variation of these quantities, considered as external parameters. More sophisticated models where the internal level structure of the emitters is explicitly taken into account were developed in [23–25] but the complexity of such a description goes far beyond the scope of the present work.

For the sake of simplicity, the strong pulse is assumed to propagate across the medium at a constant speed and to maintain a constant shape in space. We also restrict our description to a one-dimensional geometry where light modes propagate parallel to the direction of the pulse velocity. The refractive index jump is assumed to be localized at the sharp interface between two asymptotic homogeneous regions. More general configurations with smooth refractive index profiles will be the subject of future work.

A. The field equation

In the laboratory reference frame, the Lagrangian density in one dimension of the electromagnetic field coupled to N polarization fields P_i is

$$\mathcal{L}_l = \frac{(\partial_T A)^2}{8\pi c^2} - \frac{(\partial_X A)^2}{8\pi} + \sum_{i=1}^N \left(\frac{(\partial_T P_i)^2}{2\beta_i \Omega_i^2} - \frac{P_i^2}{2\beta_i} + \frac{1}{c} A \partial_T P_i \right) \quad (1)$$

where A and P_i oscillate in a direction orthogonal to their propagation direction. In this simple model the polarization is described by fields of harmonic oscillators, with strength β_i^{-1} and inertia $(\beta_i \Omega_i^2)^{-1}$. For the sake of simplicity, in this paper we shall restrict to the case $N = 3$, which suitably describes the dispersion relation in fused silica, the material used in the experiment of Ref. [9].

A propagating strong light pulse causes a local perturbations of the parameters β_i and Ω_i . Consequently, the system is stationary when observed in the reference frame comoving with the pulse at velocity v . Thus, it is convenient to transform the laboratory coordinates X and T to the comoving coordinates x and t , by applying a Lorentz boost Λ with velocity v

$$\begin{cases} t = \gamma[T - vX/c^2], \\ x = \gamma[X - vT], \end{cases} \quad (2)$$

where $\gamma = 1/\sqrt{1 - v^2/c^2}$. Coherently, differential operators transform as

$$\begin{cases} \partial_T = \gamma[\partial_t - v\partial_x], \\ \partial_X = \gamma[\partial_x - v\partial_t/c^2], \end{cases} \quad (3)$$

Furthermore, we shall treat A and P_i as scalar fields, i.e., we do not transform them under the boost. Although this might appear not correct, it is completely legitimate, as shown in Appendix A.

The transformed Lagrangian density is

$$\mathcal{L} = \frac{\dot{A}^2}{8\pi c^2} - \frac{A'^2}{8\pi} + \sum_{i=1}^3 \left[\frac{\gamma^2}{2\beta_i \Omega_i^2} (\dot{P}_i - vP_i')^2 - \frac{P_i^2}{2\beta_i} + \frac{\gamma}{c} A (\dot{P}_i - vP_i')^2 \right], \quad (4)$$

where dot and prime denote derivation with respect to t and x , respectively.

As usual, the conjugate momenta are obtained by varying the Lagrangian

$$L = \int dx \mathcal{L} \quad (5)$$

with respect to the time derivatives of A and P_i :

$$\Pi_A = \frac{\dot{A}}{4\pi c^2}, \quad \Pi_{P_i} = \frac{\gamma^2}{\beta_i \Omega_i^2} (\dot{P}_i - vP_i') + \frac{\gamma}{c} A. \quad (6)$$

We can impose canonical commutation relations on A and P_i (see Appendix A

$$\begin{aligned} [A(x), \Pi_A(x')] &= i\hbar \delta(x - x'), \\ [P_i(x), \Pi_{P_j}(x')] &= i\hbar \delta_{ij} \delta(x - x'), \end{aligned} \quad (7)$$

and all the other commutators vanish.

The Hamiltonian density

$$\mathcal{H} = \frac{1}{2} \left[\dot{A} \Pi_A + \Pi_A \dot{A} + \sum_{i=1}^3 \left(\dot{P}_i \Pi_{P_i} + \Pi_{P_i} \dot{P}_i \right) \right] - \mathcal{L} \quad (8)$$

becomes

$$\begin{aligned} \mathcal{H} = 2\pi c^2 \Pi_A^2 + \frac{A'^2}{8\pi} + \sum_{i=1}^3 \left[\frac{\beta_i \Omega_i^2}{2\gamma^2} \left(\Pi_{P_i} - \frac{\gamma}{c} A \right)^2 \right. \\ \left. + \frac{P_i^2}{2\beta_i} + \frac{1}{2} (P'_i \Pi_{P_i} + \Pi_{P_i} P'_i) \right], \end{aligned} \quad (9)$$

and the Hamilton equations are derived by the commutators of the fields and their conjugate momenta with the Hamiltonian

$$H = \int dx \mathcal{H}. \quad (10)$$

We obtain

$$\dot{A} = 4\pi c^2 \Pi_A, \quad (11)$$

$$\dot{P}_i = \frac{\beta_i \Omega_i^2}{\gamma^2} \left(\Pi_{P_i} - \frac{\gamma}{c} A \right) + v P'_i, \quad (12)$$

$$\dot{\Pi}_A = \frac{A''}{4\pi} + \sum_{i=1}^3 \left[\frac{\beta_i \Omega_i^2}{\gamma c} \left(\Pi_{P_i} - \frac{\gamma}{c} A \right) \right], \quad (13)$$

$$\dot{\Pi}_{P_i} = -\frac{P_i}{\beta_i} + \partial_x (v \Pi_{P_i}). \quad (14)$$

Note that one might have obtained the first two equations directly from the definition of conjugate momenta (6).

It is now convenient to define the eight-dimensional vector

$$V = (A \ P_1 \ P_2 \ P_3 \ \Pi_A \ \Pi_{P_1} \ \Pi_{P_2} \ \Pi_{P_3})^T \quad (15)$$

and the matrix

$$\eta = \begin{pmatrix} 0 & I_4 \\ -I_4 & 0 \end{pmatrix}, \quad (16)$$

where I_4 is the 4×4 identity matrix. With this notation the Hamilton equations can be written in a compact form as

$$\dot{V} = \eta (\nabla_V \mathcal{H}). \quad (17)$$

Moreover, a scalar product

$$\langle V_1, V_2 \rangle = \frac{i}{\hbar} \int dx V_1^\dagger(x, t) \eta V_2(x, t) \quad (18)$$

can be defined on the set of the solutions of Eq. (17), generalized to complex values. In virtue of Eq. (17), using $\eta^2 = -I_8$, $\eta^\dagger \eta = I_8$, and the fact that the Hamiltonian density \mathcal{H} is quadratic in the fields and their momenta, this scalar product is conserved by time evolution:

$$\begin{aligned} \partial_t \langle V_1, V_2 \rangle &= \frac{i}{\hbar} \int dx \left[\partial_t (V_1^\dagger) \eta V_2 + V_1^\dagger \eta \partial_t (V_2) \right] \\ &= \frac{i}{\hbar} \int dx \left[(\nabla_V \mathcal{H})^\dagger|_{(V=V_1)} V_2 - V_1^\dagger (\nabla_V \mathcal{H})^\dagger|_{(V=V_2)} \right] = 0, \end{aligned} \quad (19)$$

Being the system stationary in the reference system comoving with the pulse, the real field V can be expanded on a basis of frequency eigenmodes V_ω :

$$V = \int_0^\infty d\omega \sum_\alpha (V_\omega^\alpha \hat{a}_\omega^\alpha + V_\omega^{\alpha*} \hat{a}_\omega^{\alpha\dagger}), \quad (20)$$

where

$$\hat{a}_\omega^\alpha = \langle V_\omega^\alpha, V \rangle, \quad (21)$$

the label α denotes various modes with the same eigenfrequency ω , and V_ω^α are properly normalized (see Appendix B) with respect to the norm induced by the scalar product defined in Eq. (18).

B. Homogeneous systems

In the asymptotic regions, far from the perturbation, the system is homogeneous and the parameters Ω_i , β_i , and v are constant both in time and space. In this situation one can chose V_ω^α as momentum eigenmodes:

$$V_\omega^\alpha(x, t) = e^{-i\omega t + ik_\alpha x} \bar{V}_\omega^\alpha, \quad (22)$$

where \bar{V}_ω^α is a vector of constant \mathbb{C} -numbers, satisfying

$$-i\omega \bar{V}_\omega^\alpha = \eta \mathcal{K}(k_\alpha) \bar{V}_\omega^\alpha, \quad (23)$$

and

$$\mathcal{K}(k_\alpha) = \begin{pmatrix} k_\alpha^2/4\pi + \sum_{i=1}^3 \beta_i \Omega_i^2/c^2 & 0 & 0 & 0 & 0 & -\beta_1 \Omega_1^2/\gamma c & -\beta_2 \Omega_2^2/\gamma c & -\beta_3 \Omega_3^2/\gamma c \\ 0 & 1/\beta_1 & 0 & 0 & 0 & -ik_\alpha v & 0 & 0 \\ 0 & 0 & 1/\beta_2 & 0 & 0 & 0 & -ik_\alpha v & 0 \\ 0 & 0 & 0 & 1/\beta_3 & 0 & 0 & 0 & -ik_\alpha v \\ 0 & 0 & 0 & 0 & 4\pi c^2 & 0 & 0 & 0 \\ -\beta_1 \Omega_1^2/\gamma c & +ik_\alpha v & 0 & 0 & 0 & \beta_1 \Omega_1^2/\gamma^2 & 0 & 0 \\ -\beta_2 \Omega_2^2/\gamma c & 0 & +ik_\alpha v & 0 & 0 & 0 & \beta_2 \Omega_2^2/\gamma^2 & 0 \\ -\beta_3 \Omega_3^2/\gamma c & 0 & 0 & +ik_\alpha v & 0 & 0 & 0 & \beta_3 \Omega_3^2/\gamma^2 \end{pmatrix} \quad (24)$$

Equation (23) can be written as

$$(i\eta \mathcal{K}(k_\alpha) - \omega I_8) \bar{V}_\omega^\alpha = 0. \quad (25)$$

which has nonvanishing solutions if and only if

$$\det(i\eta \mathcal{K}(k_\alpha) - \omega I_8) = 0. \quad (26)$$

The computation of the above determinant yields the dispersion relation

$$c^2 k_\alpha^2 = \omega^2 + \sum_{i=1}^3 \frac{4\pi \beta_i \gamma^2 (\omega + vk)^2}{1 - \gamma^2 (\omega + vk)^2 / \Omega_i^2}, \quad (27)$$

that has in general 8 solutions k_α for each value of the frequency ω .

Applying the boost of Eq. (2) to ω and k , the corresponding frequency Ω and wavenumber K , measured in the laboratory reference frame, are

$$\begin{cases} \Omega = \gamma[\omega + vk], \\ K = \gamma[k + v\omega/c^2]. \end{cases} \quad (28)$$

Equation (27) becomes

$$c^2 K^2 = \Omega^2 \left[1 + \sum_{i=1}^3 \frac{4\pi \beta_i}{1 - \Omega^2 / \Omega_i^2} \right] \quad (29)$$

which is the well-known Sellmeier dispersion relation [26, 27].

The solutions of the system (23) (eigenmodes of $i\eta \mathcal{K}$) are

$$\bar{V}_\omega^\alpha = C_\omega^\alpha \begin{pmatrix} c \\ i\beta_1 \gamma (\omega + vk_\alpha) [1 - \gamma^2 (\omega + vk)^2 / \Omega_1^2]^{-1} \\ i\beta_2 \gamma (\omega + vk_\alpha) [1 - \gamma^2 (\omega + vk)^2 / \Omega_2^2]^{-1} \\ i\beta_3 \gamma (\omega + vk_\alpha) [1 - \gamma^2 (\omega + vk)^2 / \Omega_3^2]^{-1} \\ -i\omega/4\pi c \\ \gamma [1 - \gamma^2 (\omega + vk)^2 / \Omega_1^2]^{-1} \\ \gamma [1 - \gamma^2 (\omega + vk)^2 / \Omega_2^2]^{-1} \\ \gamma [1 - \gamma^2 (\omega + vk)^2 / \Omega_3^2]^{-1} \end{pmatrix} \quad (30)$$

where the constant C_ω^α is computed in Appendix B

$$|C_\omega^\alpha|^2 = \hbar \left| c^2 k_\alpha - v \sum_{i=1}^3 \frac{4\pi \beta_i \gamma^2 (\omega - vk_\alpha)}{[1 - \gamma^2 (\omega - vk_\alpha)^2 / \Omega_i^2]^2} \right|^{-1}, \quad (31)$$

using the normalization condition

$$|\langle V_{\omega_1}^{\alpha_1}, V_{\omega_2}^{\alpha_2} \rangle| = \delta(\omega_2 - \omega_1) \delta_{\alpha_2 \alpha_1}. \quad (32)$$

The modulus is needed since some modes have negative norm, because the scalar product of Eq. (18) is not positive definite. In particular, it is possible to show (see Appendix B) that the norm of a mode is positive when its laboratory frequency Ω is positive, whereas it is negative when $\Omega < 0$, independently of the value of K . Since, for a given positive value of the comoving frequency ω , the dispersion relation (27) admits solutions for k , such that $\Omega = \gamma(\omega + vk)$ is negative, there exist modes with positive frequency ω , but negative norm. This implies that, in the expansion of the field V , the Fock operators associated with those positive- ω modes are not destruction but instead creation operators. Naming P the set of positive norm modes V_ω^α , labeled by α , and N the set of negative norm modes $V_\omega^{\tilde{\alpha}}$, labeled them by $\tilde{\alpha}$, V becomes

$$V = \int_0^\infty d\omega e^{-i\omega t} \left(\sum_{\alpha \in P} e^{+ik_\alpha x} \bar{V}_\omega^\alpha \hat{a}_\omega^\alpha + \sum_{\tilde{\alpha} \in N} e^{+ik_{\tilde{\alpha}} x} \bar{V}_\omega^{\tilde{\alpha}} \hat{a}_\omega^{\tilde{\alpha}\dagger} \right) + \text{h.c.}, \quad (33)$$

where h.c. stands for hermitian conjugate. Note that the positive frequency part of the field (i.e., evolving with $e^{-i\omega t}$) mixes creation \hat{a}_ω^α and destruction $\hat{a}_\omega^{\tilde{\alpha}\dagger}$ operators.

Using Eq. (21) and the normalization of Eq. (32) for the frequency eigenmodes V_ω^α , it is easy to check that \hat{a}_ω^β and $\hat{a}_\omega^{\beta\dagger}$ are creation and destruction operators, since their commutation relations, implied by the canonical commutators of the fields given in Eq. (7), are

$$[\hat{a}_\omega^\beta, \hat{a}_{\omega'}^{\beta'\dagger}] = i\delta(\omega - \omega') \delta_{\beta\beta'}, \quad (34)$$

where now β can indifferently belong either to P or N .

C. Matching conditions

In this paper, we consider only configuration with a single analogue black hole horizons. For the sake of simplicity we model this system with two homogeneous half-line regions (representing, respectively, the interior and the exterior of the analogue black hole) connected by a

discontinuity at $x = 0$. On the two sides of the discontinuity, the oscillator strength β_i^{-1} takes different constant values

$$\beta_i = \beta_{i,L}\theta(-x) + \beta_{i,R}\theta(x). \quad (35)$$

We also impose that the inertia $(\beta_i\Omega_i^2)^{-1}$, physically corresponding to the masses of the oscillator fields [see Eq. (1)], is the same in the two regions, i.e., Ω_i must varies accordingly to

$$\beta_{i,L}\Omega_{i,L}^2 = \beta_{i,R}\Omega_{i,R}^2. \quad (36)$$

In this optical system, the step-like profile has been proved to provide reliable result when the parameters do not vary very much between the two homogeneous regions [28]. This is indeed the case in those optical system, where the relative difference in the refractive index in the two regions is of the order of 0.1% [9] (in the following analysis, for illustrative purposes, we shall mainly use a much larger, but still quite small relative difference of 10%).

In this geometry, a frequency eigenmode V_ω^α [see Eq. (20)] can be written as

$$V_\omega^\alpha = \sum_\alpha L_\omega^\alpha V_{\omega,L}^\alpha \theta(-x) + \sum_\alpha R_\omega^\alpha V_{\omega,R}^\alpha \theta(x), \quad (37)$$

where L_ω^α and R_ω^α are constant, and $V_{\omega,L}^\alpha$ and $V_{\omega,R}^\alpha$ are frequency-momentum eigenmodes, as in Eq. (22), that is they are solutions of the field equation Eq. (17) in the homogeneous left ($x < 0$) and right ($x > 0$) regions, respectively.

The relations between L_ω^α 's and R_ω^α 's, are determined by solving the field equation in a neighborhood of $x = 0$. Writing V_ω^α of Eq. (37) in a more compact form

$$V_\omega^\alpha = V_L \theta(-x) + V_R \theta(x), \quad (38)$$

its first and second spatial derivatives are

$$V_\omega^{\alpha'} = V_L' \theta(-x) + V_R' \theta(x) + (V_R - V_L)\delta(x) \quad (39)$$

$$V_\omega^{\alpha''} = V_L'' \theta(-x) + V_R'' \theta(x) + 2(V_R' - V_L')\delta(x) + (V_R - V_L)\delta'(x). \quad (40)$$

We now put the above expressions in Eqs. (11), (12), (13), and (11), and group all the terms with $\theta(x)$, $\theta(-x)$, $\delta(x)$, and $\delta'(x)$. The terms with $\theta(x)$ and $\theta(-x)$ trivially give two sets of equations, separately satisfied by V_L and V_R in the homogeneous left and right regions. These equations are solved as in Sec. II B. For instance, Eq. (11) gives

$$\dot{A}_R = 4\pi c^2 \Pi_{A,R}, \quad \dot{A}_L = 4\pi c^2 \Pi_{A,L}. \quad (41)$$

The connection formulas between the two asymptotic regions are given instead by $\delta(x)$ and $\delta'(x)$ terms. Equation (11) does not contain any of them. Equation (12) has a term with $\delta(x)$

$$v(P_{i,R} - P_{i,L})\delta(x) = 0, \quad (42)$$

yielding

$$v[P_{i,R}(0) - P_{i,L}(0)] = 0, \quad (43)$$

which has two solutions

$$v = 0, \quad \text{or} \quad P_{i,R}(0) = P_{i,L}(0). \quad (44)$$

Thus, when $v \neq 0$, P_i 's must be continuous at $x = 0$.

Equation (13) contains a second derivative of A , generating both a term with $\delta(x)$ and one with $\delta'(x)$. The associated equations are

$$A_R(0) = A_L(0), \quad A_R'(0) = A_L'(0), \quad (45)$$

so that both A and A' are continuous in $x = 0$, that is, the magnetic field B is continuous. Consequently, because of Eq. (41), also Π_A and Π_A' are continuous in $x = 0$. Since the electric field is proportional to the time derivative of A , this implies that both E and its first spatial derivative are continuous in $x = 0$.

Finally, Eq. (14) contains the first derivative of Π_P (v is constant), generating a $\delta(x)$ term that yields

$$v = 0, \quad \text{or} \quad \Pi_{P_i,L}(0) = \Pi_{P_i,R}(0), \quad (46)$$

and, consequently, Π_{P_i} 's are continuous at $x = 0$ when $v \neq 0$.

Summarizing, we proved that

- A , Π_A , and their first and second derivatives are continuous in $x = 0$,
- if $v \neq 0$, P_i and Π_{P_i} are continuous.

To completely fix the relations between modes in the left and right regions, one must determine the matching condition of P_i' and Π_{P_i}' , and also those of P_i and Π_{P_i} if $v = 0$.

a. $v \neq 0$. The $\theta(-x)$ and $\theta(x)$ terms of Eq. (12) are

$$\begin{aligned} vP_{i,L}' &= \dot{P}_{i,L} - \frac{\beta_{i,L}\Omega_{i,L}^2}{\gamma^2} \left(\Pi_{P_i,L} - \frac{\gamma}{c} A_L \right), \\ vP_{i,R}' &= \dot{P}_{i,R} - \frac{\beta_{i,R}\Omega_{i,R}^2}{\gamma^2} \left(\Pi_{P_i,R} - \frac{\gamma}{c} A_R \right). \end{aligned} \quad (47)$$

Since A , Π_A , and $\dot{P} = i\omega P$ are continuous, and $\beta_i\Omega_i^2$ are equal on both sides of the discontinuity, Eq. (47) implies that also P_i' is continuous at $x = 0$.

Similarly, the matching condition for Π_{P_i}' is found from the $\theta(-x)$ and $\theta(x)$ terms of Eq. (14):

$$\begin{aligned} \beta_{i,L} \left(\dot{\Pi}_{P_i,L} - v\Pi_{P_i,L}' \right) &= -P_{i,L}, \\ \beta_{i,R} \left(\dot{\Pi}_{P_i,R} - v\Pi_{P_i,R}' \right) &= -P_{i,R}. \end{aligned} \quad (48)$$

By continuity of P_i

$$\beta_i \left(\dot{\Pi}_{P_i} - v\Pi_{P_i}' \right) = -P_i \quad (49)$$

is continuous at $x = 0$ and, accordingly, Π'_{P_i} is discontinuous.

The continuity of \dot{P} and P' implies that the derivative of P with respect to the laboratory time T

$$\partial_T P_i = \gamma(\dot{P}_i - vP'_i) \quad (50)$$

is continuous. Analogously, Eq. (49) implies that

$$\beta_i \partial_T \Pi_{P_i} \quad (51)$$

is continuous at $x = 0$. The physical meaning of this condition is evident when the second equation of (6) is rewritten as

$$\Pi_{P_i} = \frac{\gamma}{\beta_i \Omega_i^2} \partial_T P + \frac{\gamma}{c} A. \quad (52)$$

Differentiating with respect to T :

$$\partial_T \Pi_{P_i} = \frac{\gamma}{\beta_i \Omega_i^2} \partial_T^2 P + \frac{\gamma}{c} \partial_T A, \quad (53)$$

where we used the constancy of $\beta_i \Omega_i^2$. Multiplying both sides of this equation by β_i , using Eq. (49) in the form

$$\beta_i \partial_T \Pi_P = -\gamma P_i, \quad (54)$$

and noting that $E = -\partial_T A/c$ is the electric field, one obtains

$$\partial_T^2 P = -\Omega_i^2 P_i + \beta_i \Omega_i^2 E. \quad (55)$$

This equation describes the dynamics of a harmonic oscillator of frequency Ω_i and mass $(\beta_i \Omega_i^2)^{-1}$, which is forced by E . When the perturbation, caused by the laser pulse, passes at some $X = X_0$, at time $T = T_0 = X_0/v$, the mass $(\beta_i \Omega_i^2)^{-1}$ remains unchanged, but the oscillator frequency Ω_i changes from $\Omega_{i,R}$ to $\Omega_{i,L}$. As a consequence of Eq. (55), P and $\partial_T P$ are unchanged as the perturbation arrives at $X = X_0$, but $\partial_T^2 P$ has a finite jump, i.e., it is discontinuous at $X = X_0$ and $T = T_0$.

b. $v = 0$. In this case, Eqs. (12) and (14) simplify to

$$\begin{aligned} \dot{P}_i &= \beta_i \Omega_i^2 \left(\Pi_{P_i} - \frac{A}{c} \right), \\ \dot{\Pi}_{P_i} &= -\frac{P_i}{\beta_i}. \end{aligned} \quad (56)$$

Differentiating the first equation with respect to time, using the second equation and $E = -\dot{A}/c$:

$$\ddot{P}_i = -\Omega_i^2 P_i + \beta_i \Omega_i^2 E, \quad (57)$$

which coincides with Eq. (55) because $T = t$ when $v = 0$. Since $\beta_i \Omega_i^2 E$ is continuous at $x = 0$,

$$\ddot{P}_i + \Omega_i^2 P_i \quad (58)$$

is continuous and, for an eigenmode of frequency ω

$$(\omega^2 - \Omega_{i,L}^2) P_{i,L} = (\omega^2 - \Omega_{i,R}^2) P_{i,R} \quad (59)$$

at $x = 0$. Thus, P_i is not continuous at $x = 0$, because Ω_i is discontinuous.

Similarly, by derivating the second equation of (56) with respect to time, one obtains

$$\ddot{\Pi}_{P_i} = -\Omega_i^2 \left(\Pi_{P_i} - \frac{A}{c} \right) \quad (60)$$

which implies that

$$\frac{\ddot{\Pi}_{P_i}}{\Omega_i^2} + \Pi_{P_i} \quad (61)$$

is continuous, that is

$$\left(1 - \frac{\omega^2}{\Omega_{i,L}^2} \right) \Pi_{P_{i,L}} = \left(1 - \frac{\omega^2}{\Omega_{i,R}^2} \right) \Pi_{P_{i,R}} \quad (62)$$

at $x = 0$, and Π_{P_i} is discontinuous.

To conclude this section, it is worth checking how many constants are fixed by the matching conditions. In Eq. (37), there are 16 unknown constants L_ω^α and R_ω^α , corresponding, respectively, to the 8 solutions of the dispersion relation (27) in each of the two homogeneous asymptotic regions. Moreover, for every frequency ω , there are in general 8 global solutions V_ω^α . Thus, those constants should be constrained by 8 equations, but we found 16 matching conditions for the continuity of A , P_i , Π_A , Π_{P_i} , and of their first derivatives. The system is apparently overdetermined. However, it is possible to show that 8 constraints are redundant. In fact, the 8 continuity relations of the conjugate momenta are directly implied by the 8 relations of the fields [see, for instance, Eq. (41)].

At the end of the day, for each frequency ω , there are 16 parameters and 8 independent constraints, leaving 8 free parameters, associated with the 8 globally defined solutions of the field equation (17).

III. MODE ANALYSIS

In this section we will apply the quantum field formalism introduced in the previous section to build the global eigenmodes of the system by imposing the suitable matching conditions at the transition interface. Identification of the different in-going and out-going channels and then calculation of the S matrix describing the scattering of light at the interface will be the crucial ingredients to calculate the intensity and the spectrum of the quantum vacuum emission in the next section.

A. Asymptotic modes

A stationary system (in the reference frame comoving with the laser pulse) made of two asymptotic homogeneous regions, connected by a transition region was first investigated under a purely kinematic perspective in

Ref. [20]. In particular, it was shown that it is possible to tune the velocity of propagation of the pulse in such a way that the transition between the two asymptotic flat regions looks like an analogue black horizon.

In that analysis, only the optical branch (corresponding to optical frequencies) of the dispersion relation was considered: within this approximation, the dispersion relation admits 4 solutions of k sharing the same value of the comoving frequencies ω . Before studying the full problem, taking into account all the branches of the dispersion relation, it is worth summarizing the most relevant aspect of that analysis. In fact, the use of the Sellmeier dispersion relation introduces additional complications with respect to simpler subluminal dispersion relations usually considered in the literature [4]. In particular, the absence of a low frequency regime forbid an immediate individuation of an analogue geometry.

Assuming that the perturbation is moving in the positive x direction ($v > 0$), a frequency dependent horizon is present for a given comoving frequency ω when, on the left of the perturbation, there are only negative group velocity (measured in the comoving frame) modes, while on the right there are both negative and positive group velocity modes. In this case, light can propagate only leftward in the left region, both left- and right-ward in the right region. In analogy with black hole physics, the left and right regions correspond, respectively, to the interior and the exterior of a black hole, and, in the transition region, there is one point corresponding to a black hole horizon.

This physics is illustrated in Fig. 1, where the optical branch of the dispersion relation (27) is plotted in the comoving frame, both in the left (left panel) and in the right (right panel) regions, for a step-like pulse (top panel) moving rightward at $v = 0.66c$. In the right region the dispersion relation is given directly by Eq. (27), while in the left region (representing the interior of a propagation pulse), the refractive index has been increased by $\delta n = 0.1$. Solid (dashed) curves denote branches with positive (negative) laboratory frequency. As demonstrated in Sec. II B, they correspond to positive (negative) norm modes.

The dispersion relation is solved for a given comoving frequency ω . The arrows indicate the direction of propagation of the corresponding modes. Modes are named using the notation introduced in Sec. II. The superscript o stand for positive norm optical branch, \bar{o} for negative norm optical branch. The subscript L and R denote, respectively, modes defined in the left and right region. For outer points (right panel, $\delta n = 0$), the dispersion relation has 4 solutions. Three of them correspond to modes ($V_{\omega,R}^o$, $V_{\omega,R}^{\bar{o}}$, $V_{\omega,R}^{o2}$) propagating leftward from $x = +\infty$ toward the horizon. The fourth one, denoted by an empty dot, corresponds instead to an outgoing mode ($V_{\omega,R}$), with positive group velocity. For inner points (left panel, $\delta n > 0.1$) the dispersion relation has only 2 real solutions, both corresponding to leftgoing modes ($V_{\omega,L}^{\bar{o}}$, $V_{\omega,L}^o$) which propagate from the horizon toward $x = -\infty$. Note

that the two solutions present only in the right region for $\omega_{\min} < \omega < \omega_{\max}$ correspond, respectively, to a left- ($V_{\omega,R}^{o2}$) and a right-going ($V_{\omega,R}$) mode.

As a result, according to the above given definition, within the frequency range $\omega_{\min} < \omega < \omega_{\max}$ (where $\hbar\omega_{\min}$ and $\hbar\omega_{\max}$ are represented in the right panel with dotted lines), the discontinuity in the pulse profile represent an analogue black hole horizon. Nota that there is one negative norm mode $V_{\omega,R}^{\bar{o}}$, leftward propagating from $+\infty$ to the horizon, and one solution (right panel, empty dot), corresponding to a mode $V_{\omega,R}$ propagating from the horizon to infinity in the exterior part of the analogue black hole. This mode structure might originate some phenomenon similar to Hawking radiation.

In the present paper, this analysis is extended to the full Sellmeier dispersion relation, which in general admits 8 solutions, corresponding to 8 (propagating if k is real) asymptotic modes (AM) in each region ($x < 0$ or $x > 0$). Proceeding in analogy with Ref. [20], one must first identify a range of frequencies $\omega_{\min} < \omega < \omega_{\max}$, for which the optical branch possesses 4 real solutions in the region and 2 in the left one. Second, on each side one must localize 4 additional solutions on the other branches of the dispersion relation and describe the associated modes.

In Fig. 2 the full Sellmeier dispersion relation is plotted for $x < 0$ (upper left panel) and $x > 0$ (upper right panel) in the laboratory reference frame (Ω, K) [see Eq. (29)]. A boost is then performed on the axes and the new axes (ω, k) in the reference frame comoving with the pulse are drawn [see Eq. (27)]. The central region of those plots (gray dot-bordered square) is zoomed in the bottom panels. The dispersion relation is graphically solved for a fixed value of the comoving frequency ω (dashed line), with $\omega_{\min} < \omega < \omega_{\max}$. There are 8 branches: 4 with positive Ω (solid curves) and 4 with negative Ω (dashed curves), symmetrically placed in the lower plane. In this configuration ω is small enough that no solution belongs to the highest (positive or negative) energy branches. We therefore name only the 6 branches of the dispersion relation with low energy $|\Omega|$. In the upper plane ($\Omega > 0$), starting from the lowest energy branch we call them lower (l), optical (o) and upper (u). Symmetrically, the 3 branches with negative laboratory frequency Ω and negative norm (as demonstrated in Sec. II C) are labeled by \bar{l} , \bar{o} , and \bar{u} . Accordingly, the solutions of the dispersion relation are labeled by a superscript l, o, u, \bar{l} , \bar{o} , and \bar{u} . To ease the reader the comparison with Fig. 1, the solutions on the positive and negative frequency branches o and \bar{o} are denoted by an empty dot. The arrow above each solution indicates the direction of propagation (group velocity in the comoving frame) of the associated mode $V_{\omega,L/R}^{\alpha/\bar{\alpha}}$.

Note that, for $x < 0$ (left panels), there are 6 real- k solutions, all corresponding to leftgoing modes. The remaining two solutions of Eq. (27) have complex conjugate k . They are associated with exponentially growing ($V_{\omega,L}^{\text{grow}}$) and decaying ($V_{\omega,L}^{\text{dec}}$) modes for $x \rightarrow -\infty$. For

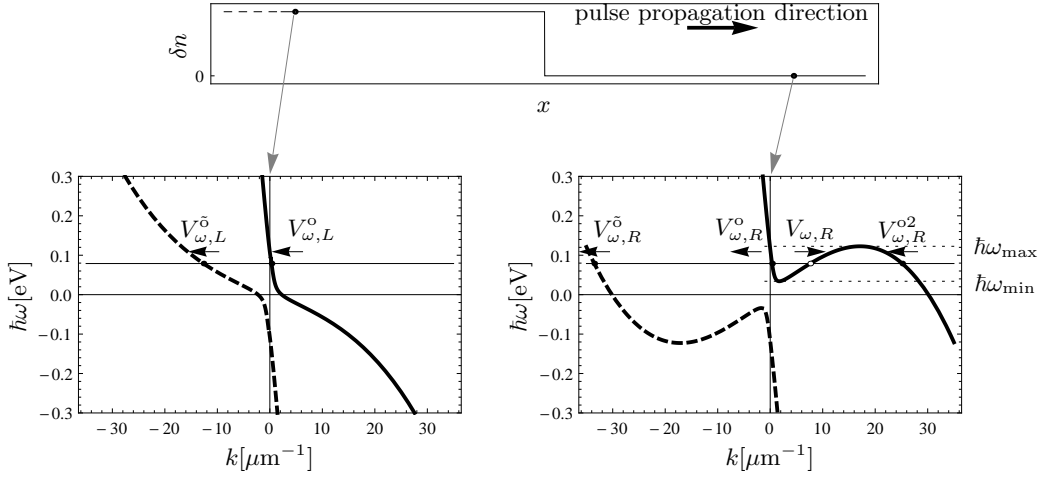


FIG. 1. Simplified analysis of the Sellmeier dispersion relation (27) in fused silica, as seen from the comoving frame. Only the optical branch is shown. Positive (negative) laboratory frequency branches are represented by solid (dashed) curves. The dispersion is plotted on the left ($\delta n = 0.001$, left panel) and on the right of a perturbation ($\delta n = 0$, right panel) moving rightward with $V = 0.66c$ in the laboratory frame (see top panel). The black horizontal line represents a generic frequency for which there are 4 real solutions in the right region (right panel), 2 real solutions in the left one (left panel), and the system shows an analogue black hole horizon. In the right panel, the dashed horizontal lines indicate the maximum and the minimum values of the frequency for which this behavior occurs. Modes are labeled with the notation introduced in Sec. II and their propagation direction is indicated by arrows.

$x > 0$ (right bottom panel), instead, the 8 solutions are all real. The two extra real solutions, that do not have a corresponding solution on the left side, belong to the optical branch and are associated, respectively, with a left-going mode, named $V_{\omega,R}^{o2}$, and with the unique rightgoing mode, simply named $V_{\omega,R}$, without any superscript.

B. Globally defined modes

In the previous section, plane waves modes propagating in the asymptotically flat left and right regions have been identified. Combining those asymptotic waves, two relevant bases of globally defined asymptotically bounded modes (GDMs) (not diverging at infinity) can be constructed.

We define the *in* basis as the set of *in* modes, whose asymptotic decomposition (37) has only one AM with group velocity v_g directed toward $x = 0$. We say that the group velocity of an AM is directed toward the horizon if $v_g > 0$ ($v_g < 0$) for modes which are solution of the mode equation in the left (right) region.

Analogously, we define the *out* basis as the set of *out* modes, whose asymptotic decomposition have only one AM with group velocity directed toward $x = -\infty$ ($x = +\infty$), if the AM is a solution of the field equation in the left (right) region.

To clarify the meaning of these definitions with an example, the asymptotic decomposition of one of the three negative norm *in* GDMs is schematically represented in Fig. 3. We name it $V_{\omega,R}^{\text{in},\bar{o}}$, since its unique incoming AM is $V_{\omega,R}^{\bar{o}}$, that is $R_{\omega}^{\bar{o}}$ is the only non-vanishing coefficient as-

sociated with a mode with group velocity directed toward the horizon, in the asymptotic decomposition of Eq. (37) (see also Fig. 2).

In Table I, all the coefficients L_{ω}^{α} 's and R_{ω}^{α} 's are reported for the asymptotic decompositions of the three negative norm *in* GDMs $V_{\omega}^{\text{in},\bar{l}}$, $V_{\omega}^{\text{in},\bar{o}}$, $V_{\omega}^{\text{in},\bar{u}}$. As noticed in the previous section, both the AMs $V_{\omega,R}^{o2}$ and $V_{\omega,R}$, which are present only in the right region, lie on the optical branch of the dispersion relation. As mention at the beginning of Sec. III A, in the simplified analysis restricted to the optical branch, analogue Hawking radiation is expected on the AM $V_{\omega,R}$, due to the scattering at the analogue horizon of the optical negative-norm incoming GDM $V_{\omega}^{\text{in},\bar{o}}$. Thus, aiming to extend the definition of Hawking radiation to the present situation, adopting standard notation, we name β_{ω} the coefficient of $V_{\omega,R}$ in the expansion of $V_{\omega}^{\text{in},\bar{o}}$. Similarly, we name α_{ω} the coefficient of $V_{\omega,L}^{\bar{o}}$. Furthermore, adopting the notation of Ref. [29], the coefficients of modes with negative (positive) norm, in the expansion of modes with negative norm are named A (B). As an example, in the expansion of the negative norm mode $V_{\omega}^{\text{in},\bar{o}}$, the coefficients of the negative norm modes $V_{\omega,L}^{\bar{l}}$ and $V_{\omega,L}^{\bar{u}}$ are named $A_{\omega}^{o,l}$ and $A_{\omega}^{o,u}$. The coefficients of the positive norm modes $V_{\omega,L}^{\bar{o}}$, $V_{\omega,L}^{\bar{l}}$, and $V_{\omega,L}^{\bar{u}}$ are named B_{ω} , $B_{\omega}^{o,l}$, and $B_{\omega}^{o,u}$, respectively.

Finally, the 8 unknown coefficients in the two left and right asymptotic expansions for each GDM are determined by imposing the matching conditions (8 independent equations), derived in Sec. II C.

By proceeding along this line, it is possible to construct 7 *in* GDMs: $V_{\omega}^{\text{in},\bar{l}}$, $V_{\omega}^{\text{in},\bar{o}}$, $V_{\omega}^{\text{in},\bar{u}}$, $V_{\omega}^{\text{in},l}$, $V_{\omega}^{\text{in},o}$, $V_{\omega}^{\text{in},u}$,

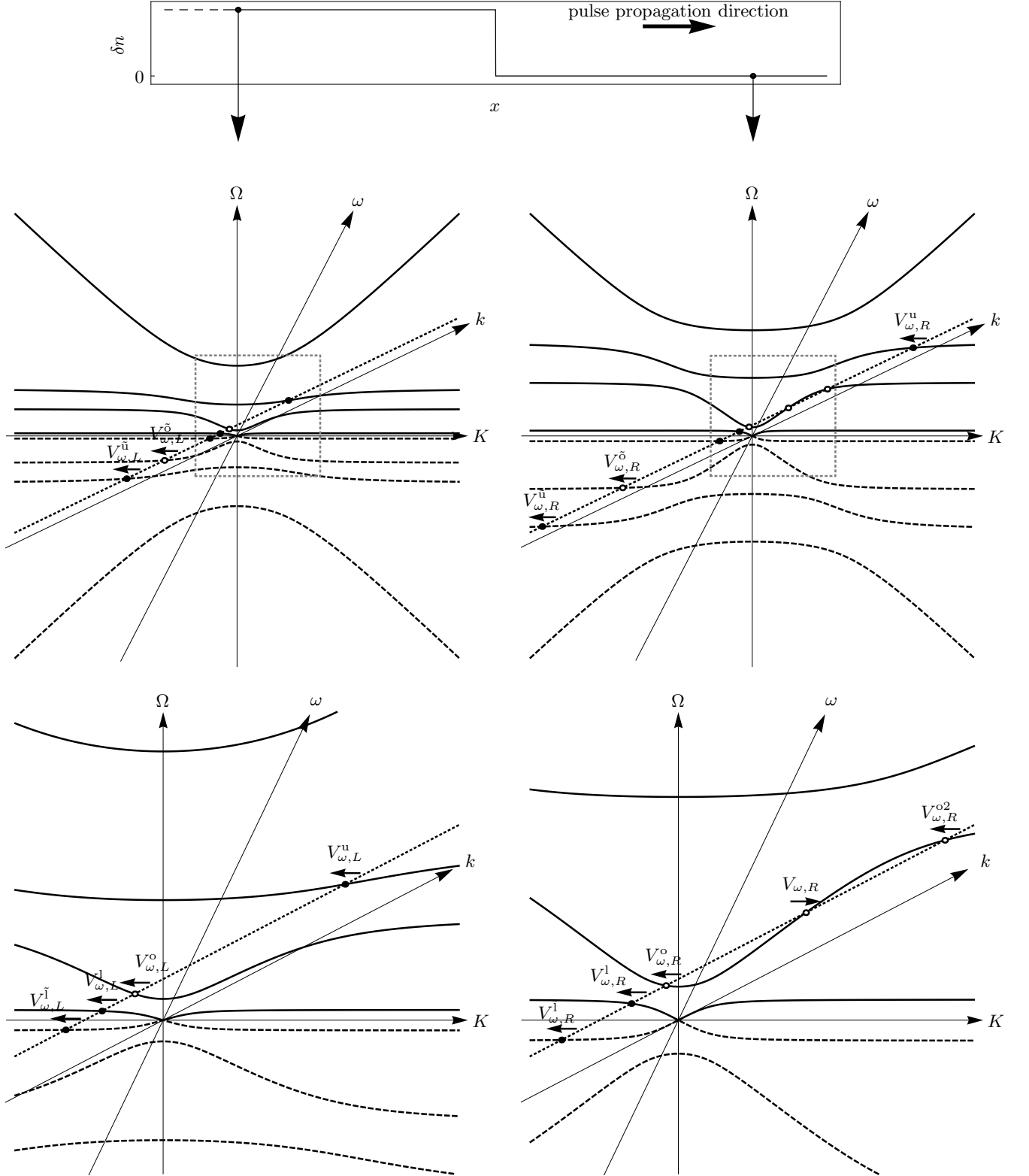


FIG. 2. Graphical representation of the Sellmeier dispersion relation, as seen from the laboratory reference frame (Ω, K) , for $x < 0$ (left panels) and $x > 0$ (right panels). The (ω, k) axes of the comoving reference frame are obtained through a boost of velocity v . As sketched in the top panel, the refractive index in the left region is larger than in the right region. This difference in the refractive index is obtained by properly changing the parameters β_i and Ω_i appearing in the Lagrangian (1). In this plot the values of the velocity v and of the refractive index change δn have been arbitrarily chosen for illustrative purposes. The bottom panels are zoom of the gray dot-bordered squared of the respective upper panels. The dispersion relation is graphically solved for a fixed comoving frequency ω , chosen in the frequency window in which the black hole horizon is present. Solutions appear both on the positive-norm positive- Ω branches (solid curves) and on the negative-norm negative- Ω branches (dashed curves). The empty dots denote solutions on the optical branches with positive (o) and negative (\bar{o}) frequency Ω . The arrows indicate the direction of propagation (group velocity in the comoving frame) of the associated modes $V_{\omega,L/R}^{\alpha/\bar{\alpha}}$. In the left region (left panels), the dispersion relation has only 6 real- k solutions. In the right region (right panels), the real- k solutions are 8,

	Coefficients of left modes									Coefficients of right modes							
	$V_{\omega,L}^{\bar{1}}$	$V_{\omega,L}^{\bar{o}}$	$V_{\omega,L}^{\bar{u}}$	$V_{\omega,L}^1$	$V_{\omega,L}^o$	$V_{\omega,L}^u$	$V_{\omega,L}^{\text{dec}}$	$V_{\omega,L}^{\text{grow}}$		$V_{\omega,R}^{\bar{1}}$	$V_{\omega,R}^{\bar{o}}$	$V_{\omega,R}^{\bar{u}}$	$V_{\omega,R}^1$	$V_{\omega,R}^o$	$V_{\omega,R}^{o2}$	$V_{\omega,R}^u$	$V_{\omega,R}$
$V_{\omega}^{\text{in},\bar{1}}$	α_{ω}^1	$A_{\omega}^{1,o}$	$A_{\omega}^{1,u}$	B_{ω}^1	$B_{\omega}^{1,o}$	$B_{\omega}^{1,u}$	D_{ω}^1	0		1	0	0	0	0	0	0	β_{ω}^1
$V_{\omega}^{\text{in},\bar{o}}$	$A_{\omega}^{o,1}$	α_{ω}	$A_{\omega}^{o,u}$	$B_{\omega}^{o,1}$	B_{ω}	$B_{\omega}^{o,u}$	D_{ω}^o	0		0	1	0	0	0	0	0	β_{ω}
$V_{\omega}^{\text{in},\bar{u}}$	$A_{\omega}^{u,1}$	$A_{\omega}^{u,o}$	α_{ω}^u	$B_{\omega}^{u,1}$	$B_{\omega}^{u,o}$	B_{ω}^u	D_{ω}^u	0		0	0	1	0	0	0	0	β_{ω}^u

TABLE I. Coefficients of the asymptotic decomposition of the globally defined *in* modes $V_{\omega}^{\text{in},\bar{1}}$, $V_{\omega}^{\text{in},\bar{o}}$, and $V_{\omega}^{\text{in},\bar{u}}$ on the bases of left and right AMs.

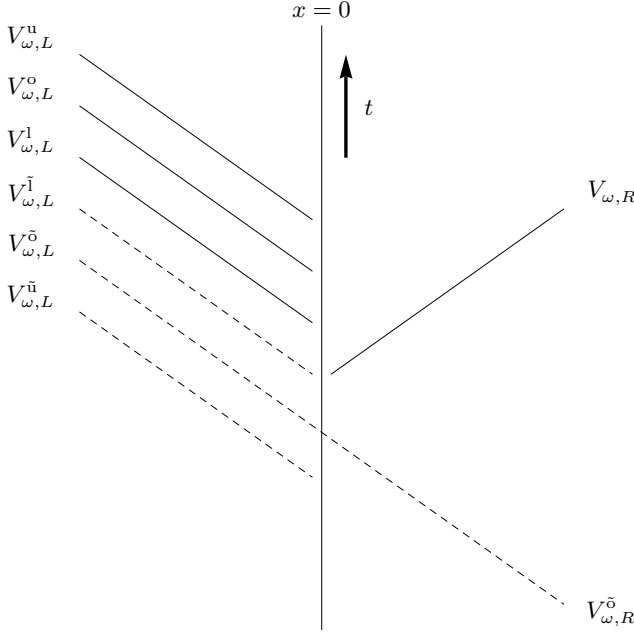


FIG. 3. Asymptotic decomposition of the globally defined *in* mode $V_{\omega}^{\text{in},\bar{o}}$. The only asymptotic branch with group velocity directed toward the horizon is $V_{\omega,R}^{\bar{o}}$. Positive (negative) norm modes are represented by solid (dashed) lines.

$V_{\omega}^{\text{in},o2}$, whose unique branches with group velocity directed toward the horizon are, respectively, $V_{\omega,R}^{\bar{1}}$, $V_{\omega,R}^{\bar{o}}$, $V_{\omega,R}^{\bar{u}}$, $V_{\omega,R}^1$, $V_{\omega,R}^o$, $V_{\omega,R}^u$, $V_{\omega,R}^{o2}$. Similarly, one constructs 7 *out* GDMs: $V_{\omega}^{\text{out},\bar{1}}$, $V_{\omega}^{\text{out},\bar{o}}$, $V_{\omega}^{\text{out},\bar{u}}$, $V_{\omega}^{\text{out},1}$, $V_{\omega}^{\text{out},o}$, $V_{\omega}^{\text{out},u}$, V_{ω}^{out} , whose unique branches with group velocity directed to infinity are, respectively, $V_{\omega,L}^{\bar{1}}$, $V_{\omega,L}^{\bar{o}}$, $V_{\omega,L}^{\bar{u}}$, $V_{\omega,L}^1$, $V_{\omega,L}^o$, $V_{\omega,L}^u$, $V_{\omega,L}$.

C. The scattering matrix

As in Eq. (33), the field operator V is expanded indifferently with respect either to the *in* or to the *out* basis

of GDMs.

$$V = \int_0^\infty d\omega e^{-i\omega t} \left(\sum_{\alpha \in P} V_{\omega}^{\text{in},\alpha} \hat{a}_{\omega}^{\text{in},\alpha} + \sum_{\tilde{\alpha} \in N} V_{\omega}^{\text{in},\tilde{\alpha}} \hat{a}_{\omega}^{\text{in},\tilde{\alpha}\dagger} \right) + \text{h.c.} \quad (63)$$

$$= \int_0^\infty d\omega e^{-i\omega t} \left(\sum_{\alpha \in P} V_{\omega}^{\text{out},\alpha} \hat{a}_{\omega}^{\text{out},\alpha} + \sum_{\tilde{\alpha} \in N} V_{\omega}^{\text{out},\tilde{\alpha}} \hat{a}_{\omega}^{\text{out},\tilde{\alpha}\dagger} \right) + \text{h.c.}, \quad (64)$$

The transformation between the two bases follows straightforwardly from the construction of the previous section. In fact, since the two bases of *in* and *out* GDMs, the basis of left AMs and the basis of right AMs are all orthogonal, the coefficients of the matrix connecting the *in* and *out* modes can be directly read from the expansion of *in* and *out* modes on AMs. For instance, from the second line of Table I:

$$V_{\omega}^{\text{in},\bar{o}} = A_{\omega}^{o,1} V_{\omega}^{\text{out},\bar{1}} + \alpha_{\omega} V_{\omega}^{\text{out},\bar{o}} + A_{\omega}^{o,u} V_{\omega}^{\text{out},\bar{u}} + B_{\omega}^{o,1} V_{\omega}^{\text{out},1} + B_{\omega} V_{\omega}^{\text{out},o} + B_{\omega}^{o,u} V_{\omega}^{\text{out},u} + \beta_{\omega} V_{\omega}^{\text{out}}. \quad (65)$$

Repeating this procedure for each *in* mode, the scattering matrix S is fully determined

$$V_{\omega}^{\text{in},\beta} = \sum_{\beta'} S^{\beta\beta'} V_{\omega}^{\text{out},\beta'}, \quad (66)$$

where β and β' run over all positive and negative norm modes. The relation between *in* and *out* destruction and creation operators is easily derived from the S matrix:

$$\hat{A}^{\text{out}} = S^T \hat{A}^{\text{in}}, \quad (67)$$

where \hat{A}^{in}

$$\hat{A}^{\text{in}} = \left(\hat{a}_{\omega}^{\text{in},\bar{1}\dagger} \hat{a}_{\omega}^{\text{in},\bar{o}\dagger} \hat{a}_{\omega}^{\text{in},\bar{u}\dagger} \hat{a}_{\omega}^{\text{in},1} \hat{a}_{\omega}^{\text{in},o} \hat{a}_{\omega}^{\text{in},u} \hat{a}_{\omega}^{\text{in},o2} \right)^T \quad (68)$$

$$\hat{A}^{\text{out}} = \left(\hat{a}_{\omega}^{\text{out},\bar{1}\dagger} \hat{a}_{\omega}^{\text{out},\bar{o}\dagger} \hat{a}_{\omega}^{\text{out},\bar{u}\dagger} \hat{a}_{\omega}^{\text{out},1} \hat{a}_{\omega}^{\text{out},o} \hat{a}_{\omega}^{\text{out},u} \hat{a}_{\omega}^{\text{out}} \right)^T \quad (69)$$

are 7-dimensional vector formed, respectively, by the *in* and *out* creation operators $\hat{a}_{\omega}^{\text{in},\tilde{\alpha}\dagger}$ and $\hat{a}_{\omega}^{\text{in},\tilde{\alpha}\dagger}$ of the negative norm modes, and by the *in* and *out* destruction operators $\hat{a}_{\omega}^{\text{in},\alpha}$ and $\hat{a}_{\omega}^{\text{out},\alpha}$ of the positive norm modes.

IV. SPONTANEOUS EMISSION

In this section we shall make use of the S matrix calculated in the previous section to provide quantitative predictions for observable quantities such as the intensity and the spectrum of the quantum vacuum emission. A straightforward extension of the formalism following the lines of [30, 31] can be used to obtain information on the correlation properties of the emitted quantum vacuum emission into the different out-going modes: given the importance of correlation experiments to assess the quantum vacuum nature of the emission, this problem will be the subject of future work.

A. Comoving frame

For the sake of simplicity, we make the reasonable assumption that there are no ingoing particles, i.e., the system is in the Fock vacuum state defined by the destruction operators associated with the *in* modes:

$$\hat{a}_{\omega}^{\text{in},\alpha}|0_{\text{in}}\rangle = 0, \quad \hat{a}_{\omega}^{\text{in},\bar{\alpha}}|0_{\text{in}}\rangle = 0. \quad (70)$$

The occupation numbers of *out* modes on this state are easily computed using Eq. (67). They in general do not vanish, since Eq. (67) mixes creation and destruction operators. For instance, the expected occupation number of the unique rightgoing mode V_{ω}^{out} on the state $|0_{\text{in}}\rangle$ is

$$\langle 0_{\text{in}}|2\pi\hat{a}_{\omega}^{\text{out}\dagger}\hat{a}_{\omega}^{\text{out}}|0_{\text{in}}\rangle = 2\pi\delta(0)(|\beta_{\omega}|^2 + |\beta_{\omega}^{\text{l}}|^2 + |\beta_{\omega}^{\text{u}}|^2), \quad (71)$$

where the factor 2π has been inserted coherently with the normalization of the Fock operators of Eq. (34). As usual, there is an infrared divergence associated with the quantization of a field theory in an infinite spacetime volume. Going to a finite size time-box Δt , one must replace

$$2\pi\delta(\omega - \omega') \longrightarrow \Delta t \delta_{\omega\omega'}. \quad (72)$$

This implies that the number of particles Δn created in a time Δt at a frequency ω is

$$\Delta n_{\omega}^{\text{out}} = (|\beta_{\omega}|^2 + |\beta_{\omega}^{\text{l}}|^2 + |\beta_{\omega}^{\text{u}}|^2)\Delta t. \quad (73)$$

Analogously, there are several other channels in which particles are created, related to the mixing of the other positive and negative norm modes. For the positive frequency modes one obtains

$$\Delta n_{\omega}^{\text{out},\text{l}} = (|B_{\omega}^{\text{l}}|^2 + |B_{\omega}^{\text{o},\text{l}}|^2 + |B_{\omega}^{\text{u},\text{l}}|^2)\Delta t, \quad (74)$$

$$\Delta n_{\omega}^{\text{out},\text{o}} = (|B_{\omega}^{\text{o}}|^2 + |B_{\omega}^{\text{l},\text{o}}|^2 + |B_{\omega}^{\text{u},\text{o}}|^2)\Delta t, \quad (75)$$

$$\Delta n_{\omega}^{\text{out},\text{u}} = (|B_{\omega}^{\text{u}}|^2 + |B_{\omega}^{\text{l},\text{u}}|^2 + |B_{\omega}^{\text{o},\text{u}}|^2)\Delta t. \quad (76)$$

Since in the comoving reference frame, the source of photons (the pulse) is at rest, the number of created particles r_{ω} per unit time and unit bandwidth coincides with

the flux of particles I_{ω} crossing a certain surface at constant x . Thus, the flux of particles per unit time and unit bandwidth in the comoving reference frame is

$$I_{\omega}^{\text{out},\alpha} = r_{\omega}^{\text{out},\alpha} = \frac{dn_{\omega}^{\text{out},\alpha}}{dt d\omega} = \frac{\Delta n_{\omega}^{\text{out},\alpha}}{\Delta t}. \quad (77)$$

The flux of energy (which coincides with the energy production rate in the reference frame where the source is at rest) associated with the mode α is

$$f_{\omega}^{\text{out},\alpha} = \frac{dE_{\omega}^{\text{out},\alpha}}{dt d\omega} = \hbar\omega I_{\omega}^{\text{out},\alpha}. \quad (78)$$

In Fig. 4 we plot the fluxes of particles I_{ω}^{out} (solid line), $I_{\omega}^{\text{out},\text{l}}$ (dashed line), $I_{\omega}^{\text{out},\text{o}}$ (dotted line), $I_{\omega}^{\text{out},\text{u}}$ (dot-dashed line) and the respective energy fluxes (right panel) f_{ω}^{out} , $f_{\omega}^{\text{out},\text{l}}$, $f_{\omega}^{\text{out},\text{o}}$, and $f_{\omega}^{\text{out},\text{u}}$, for a pulse moving with velocity $v = 0.66c$. The values of $\beta_{i,R}$ and $\Omega_{i,R}$ in the right region have been chosen accordingly to the dispersion relation in fused silica, the material used in the experiment of Ref. [9]:

$$\begin{aligned} \beta_{1,R} &= 0.07141914, & \hbar\Omega_{1,R} &= 0.125285 \text{ eV}, \\ \beta_{2,R} &= 0.03246304, & \hbar\Omega_{2,R} &= 10.6661 \text{ eV}, \\ \beta_{3,R} &= 0.05539915, & \hbar\Omega_{3,R} &= 18.1252 \text{ eV}. \end{aligned} \quad (79)$$

In the left region, for illustrative purposes we used

$$\beta_{i,L} = (1 + \epsilon)\beta_{i,R}, \quad \Omega_{i,L} = (1 + \epsilon)^{-1/2}\Omega_{i,R}, \quad (80)$$

with a very large value of $\epsilon = 0.3$. When Ω is in the optical range and far enough from the poles of the dispersion relation

$$\delta n_L - n_R \approx \frac{n_R^2 - 1}{2n_R}\epsilon, \quad (81)$$

that yields a quite large value of $\delta n \approx 0.12$, which requires a very strong laser intensity $I \approx 3 \times 10^{14} \text{ W/cm}^2$ [9, 20].

From Fig. 4, the dominant contribution to the energy flux comes from the rightgoing modes, corresponding to a Hawking-like process, in the sense discussed in the previous section and in Ref. [20]. What can we say about its thermal properties? It is well known that, the thermal energy flux in 1+1 dimension is exactly constant in the limit $\omega \rightarrow 0$. In the present situation, however, this channel is open only in a narrow range of frequencies $\omega_{\text{min}} < \omega < \omega_{\text{max}}$ (see Fig. 1), and the low frequency limit cannot be taken. Therefore, asking whether the spectrum is thermal or not is not really a well-posed question. Nevertheless, one may observe that the energy flux is almost constant, far from the boundary values ω_{min} and ω_{max} . This is all what is possible to say about the thermal properties of this spectrum.

To investigate more deeply the features of the spectrum of V_{ω}^{out} (the global modes associated with the asymptotic plane wave $V_{\omega,R}$, see Fig. 2), in Fig. 5 the flux of particles is separated into their components due to $|\beta_{\omega}|^2$

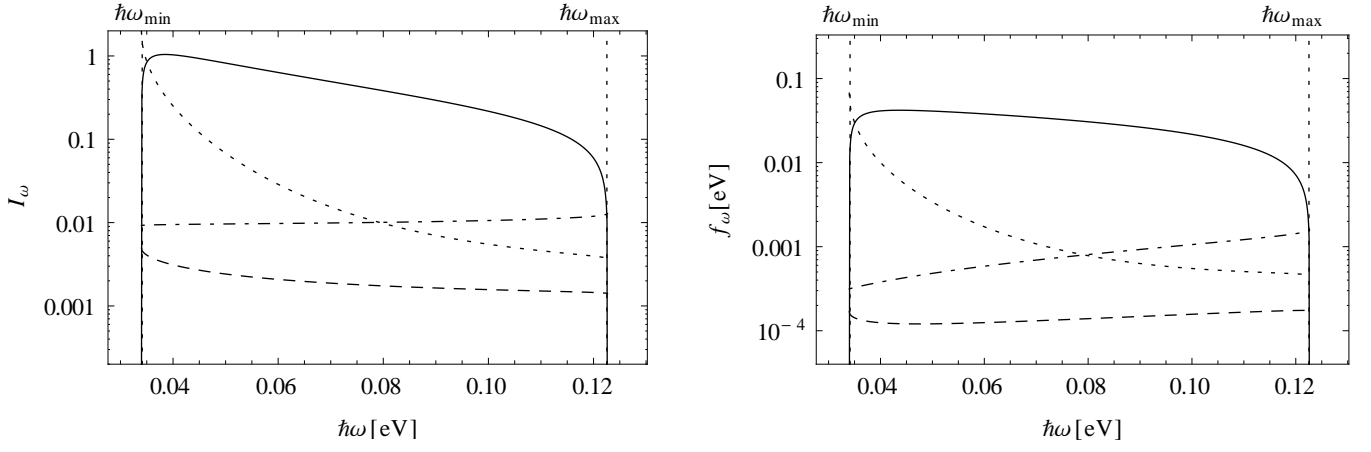


FIG. 4. Particle fluxes (left panel) I_ω^{out} (solid line), $I_\omega^{\text{out},l}$ (dashed line), $I_\omega^{\text{out},o}$ (dotted line), $I_\omega^{\text{out},u}$ (dot-dashed line) and the corresponding energy fluxes (right panel) f_ω^{out} , $f_\omega^{\text{out},l}$, $f_\omega^{\text{out},o}$, and $f_\omega^{\text{out},u}$ as seen from the comoving reference frame, for a horizon configuration, as sketched in Fig. 2. Parameters $v = 0.66c$ and $\epsilon = 0.3$, yielding via Eq. (80) a refractive index jump of $\delta n = 0.12$ for optical frequencies.

(solid line), $|\beta_\omega^l|^2$ (dashed line) and $|\beta_\omega^u|^2$ (dotted line). Note that the contributions to spontaneous emission on the mode V_ω^{out} by the lower and the upper branch are negligible with respect to the term coming from the optical negative frequency mode $V_\omega^{\text{in},\bar{o}}$, associated with the asymptotic mode $V_{\omega,R}^{\bar{o}}$ of Fig. 2. This behavior was predicted and justified in Ref. [20] and it has been now confirmed by the present calculation.

B. Laboratory frame

One may wonder what are the spectral features as measured in the laboratory reference frame. Note that, the relevant experimental quantity is not the flux of particles but the total number of particles created by the moving pulse. In fact, the pulse stably propagates only for a very

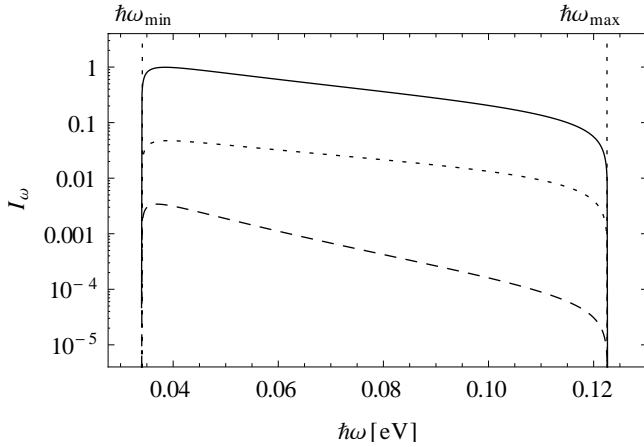


FIG. 5. Separate contribution of $|\beta_\omega|^2$ (solid line), $|\beta_\omega^l|^2$ (dashed line) and $|\beta_\omega^u|^2$ (dotted line) to the flux of particles I_ω^{out} , for the horizon configuration considered in Fig. 4.

short distance ΔX_s (about 1 mm [10]), corresponding to a duration of $\Delta T_s = \Delta X_s/V_g$. In an experiment one observes the pulse in this small region and measures the photons produced therein. Naming R_Ω the production rate of particles at frequency Ω , as measured in the laboratory, the number of particles produced by the pulse in the laboratory time dT , in the range of frequency $(\Omega, \Omega + d\Omega)$ is

$$\Delta N = R_\Omega dT d\Omega. \quad (82)$$

Since the number of created particles is invariant under Lorentz transformation

$$\Delta N = r_\Omega dt d\omega. \quad (83)$$

that is ΔN can also be computed as the number of particle created in the comoving time dt by the pulse, in the frequency range $(\omega, \omega + d\omega)$. To compute the relation between R_Ω and r_ω , it is enough to compute the transformation rules of the frequency range and of the time interval. Using the inverse of the Lorentz transformation (28)

$$\omega = \gamma(\Omega - vK) \quad (84)$$

$d\omega$ can be expressed in term of $d\Omega$ as

$$d\omega = \gamma \left(d\Omega - v \frac{dK}{d\Omega} d\Omega \right) = \gamma \left(1 - \frac{v}{V_g(\Omega)} \right) d\Omega, \quad (85)$$

where V_g is the particle group velocity measured in the laboratory reference frame. The transformation of the time interval is found by noting that the source (the pulse) is at rest in the comoving frame, so dt is its proper time interval. Consequently the corresponding laboratory time interval dT is given by the usual Lorentz dilation of time

$$dT = \gamma dt. \quad (86)$$

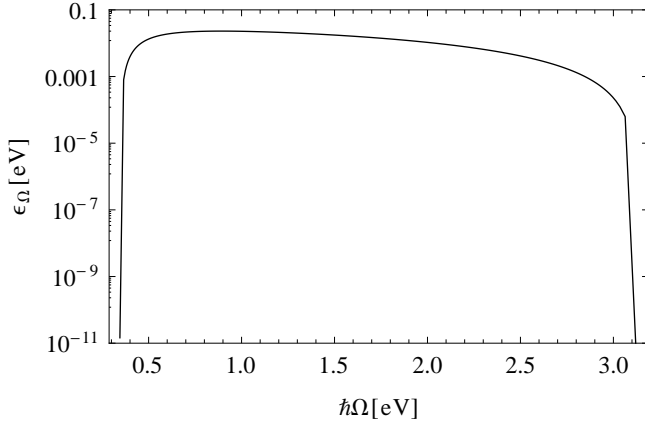


FIG. 6. Energy production rate $\varepsilon_{\Omega}^{\text{out}}$ on the rightgoing mode $V_{\omega(\Omega)}^{\text{out}}$ as seen by an observer in the laboratory, for the horizon configuration considered in Fig. 4.

Putting everything together, the rate of particle production, as seen in the laboratory frame is

$$R_{\Omega} = \left(1 - \frac{v}{V_g}\right) r_{\omega}. \quad (87)$$

The corresponding energy production rate ε_{Ω} in the laboratory frame is

$$\varepsilon_{\Omega} = \hbar\Omega R_{\Omega} = \hbar\Omega I_{\Omega} \left(1 - \frac{v}{V_g}\right). \quad (88)$$

This quantity is plotted in Fig. 6 for the rightgoing mode V_{ω}^{out} . The effect of the boost is twofold. First, it shifts the emission frequency in the laboratory: Ω is much larger than the comoving frequency ω , reaching optical frequencies. Unfortunately, as observed in [20], the boost effect is lost when one looks perpendicularly to the pulse propagation in a 3-dimensional system. Radiation at such high frequency could be observed perpendicularly only if some scattering process changed the direction of photons.

To conclude this section, let us roughly estimates the number of photons emitted on the rightgoing mode $V_{\omega(\Omega)}^{\text{out}}$ by this process. Integrating in frequency the production rate in the laboratory frame and multiplying it by the time $\Delta T_s = \Delta X_s/V$ over which the pulse stably propagates, we obtain (for $\Delta X_s \approx 1$ mm)

$$N_{\text{pulse}} = \int R_{\Omega} d\Omega \frac{\Delta X_s}{V} \approx 240. \quad (89)$$

Of course, the same result can be obtained by directly integrating the particle production rate r_{ω} , measured in the comoving frame (coinciding with the flux I_{ω}), over the comoving frequency ω and multiplying by the proper duration of the pulse $\Delta t_s = \Delta T_s/\gamma(V)$.

C. Outside the analog horizon frequency window

In this section, the emission properties are investigated for comoving frequencies below ω_{\min} and above ω_{\max} , where the main particle production channel disappears. Particle creation is indeed possible also outside the $\omega_{\min} \div \omega_{\max}$ range, through the other channels and the dashed, dotted and dot-dashed lines of Fig. 4 can then be extended for $\omega < \omega_{\min}$ and $\omega > \omega_{\max}$. Since, for those values of the comoving frequency, there are only 6 real- k solutions also for $x > 0$, a new mode analysis must be performed following Sec. III to compute a new 6×6 scattering matrix. In Fig. 7 the numerical results of this computation are reported, together with the results for $\omega_{\min} < \omega < \omega_{\max}$, obtained in the previous section. The flux of particles in the comoving frame $I_{\omega}^{\text{out},l}$ (dashed line), $I_{\omega}^{\text{out},o}$ (dotted line), and $I_{\omega}^{\text{out},u}$ (dot-dashed line) are plotted in the left panel, and the respective energy fluxes f_{ω}^{out} , $f_{\omega}^{\text{out},l}$, $f_{\omega}^{\text{out},o}$, in the right one.

First, note that the emission is peaked in the frequency range $\omega_{\min} < \omega < \omega_{\max}$, thanks to the presence of the Hawking channel (solid line). This result confirms the naive expectation that the presence of horizon should enhance the production of particles.

Second, both the occupation numbers and the energy fluxes are continuous at $\omega = \omega_{\min}$ and $\omega = \omega_{\max}$, for modes that do not feel the presence of any horizon, i.e., when no turning point is present. For these modes the transition between the two regimes is continuous.

Third, it is worth remarking that the high frequency region of this plot must be read *cum grano salis*. Indeed, we used step functions to describe the spatial behavior of β_i and Ω_i , such that arbitrary large frequency/momentum modes are excited. However, in real physical situations, the transition between the two regions $x < 0$ and $x > 0$ takes place on a finite length and only modes up to a certain frequency ω_{cutoff} are excited. Thus, Fig. 7 provides reliable results only up to ω_{cutoff} . Beyond this frequency, the off-diagonal coefficients of the scattering matrix S go to zero exponentially with ω and S reduces to the identity. Indeed, for $\omega > \omega_{\text{cutoff}}$, modes do not mix because they are well approximated by their WKB expansion. In a realistic situation, ω_{cutoff} is not larger than the frequency associated with the width of the steepening of the pulse [10, 16] (approximately $1 \mu\text{m}$), corresponding to $\omega_{\text{cutoff}} \approx 2 \times 10^{15} \text{ s}^{-1}$ ($\hbar\omega_{\text{cutoff}} \approx 1.3 \text{ eV}$).

V. PARTICLE PRODUCTION IN OTHER CONFIGURATIONS

In the previous section, we derived the flux of spontaneously created particles in a configuration closely resembling a black hole geometry. However, radiation from vacuum fluctuation is expected even in optical system without horizons, provided that negative norm modes are present [20]. We now apply the techniques introduced in this paper to the horizonless configuration ex-

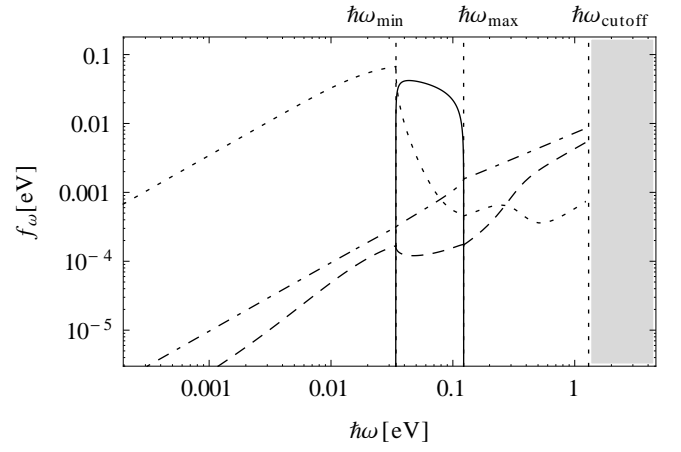
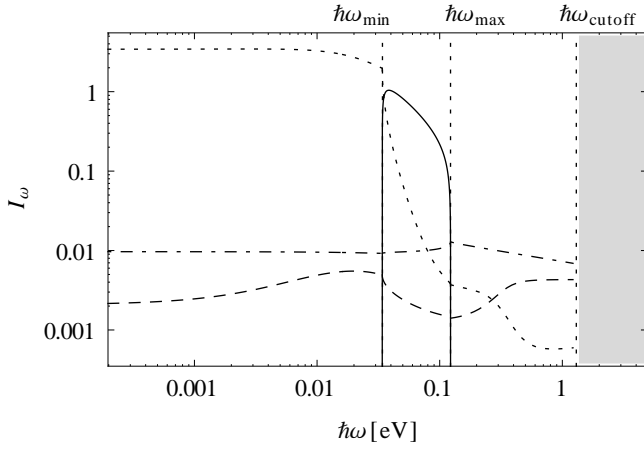


FIG. 7. Fluxes of particles I_{ω}^{out} (solid line), $I_{\omega}^{\text{out},l}$ (dashed line), $I_{\omega}^{\text{out},o}$ (dotted line), $I_{\omega}^{\text{out},u}$ (dot-dashed line) and the respective energy fluxes (right panel) f_{ω}^{out} , $f_{\omega}^{\text{out},l}$, $f_{\omega}^{\text{out},o}$, and $f_{\omega}^{\text{out},u}$, for the horizon configuration considered in Fig. 4. The plot has been cutoff at $\omega > \omega_{\text{cutoff}}$. I_{ω}^{out} and f_{ω}^{out} (solid lines) are defined only for $\omega_{\text{min}} < \omega < \omega_{\text{max}}$.

perimentally realized in Ref. [9] for a weaker perturbation ($\delta n \approx 0.001$). Indeed, outside that frequency range, the two optical modes V_{ω}^{out} and $V_{\omega}^{\text{out},o2}$ (see Fig. 2) disappear. Thus, this situation is completely analogous to a system without horizons. As a preliminary step, however, we compute the emitted flux for a horizon configuration with a value of $\delta n \approx 0.001$, which coincide with the experimental value [9], so that it is possible to compare the flux produced by a weak perturbation, both in the presence and in the absence of horizons.

A. Small refractive index jump

In a realistic situation δn is generally a couple of orders of magnitude smaller than the value above used. Unfortunately, if δn is small, the pulse velocity v must be extremely fine tuned in order to obtain a configuration with a horizon, as in Fig. 2. The frequency window ($\omega_{\text{min}}, \omega_{\text{max}}$) becomes very narrow and the emission on the rightgoing mode V_{ω}^{out} is strongly suppressed. In Fig. 8, the energy fluxes associated with the spontaneous particle production are represented for $\delta n = 0.001$. This value has been obtained by modifying the values of β_i and Ω_i in the left region, as in Eq. (80), with $\epsilon \approx 0.0026$. The pulse velocity is $v = 0.6838c$, $\hbar\omega_{\text{min}} = 0.01379 \text{ eV}$, and $\hbar\omega_{\text{max}} = 0.01396 \text{ eV}$.

The Hawking channel is not the dominant one, but its flux is now comparable with the flux of leftgoing particles on the optical-branch mode $V_{\omega}^{\text{out},o}$. In Fig. 9, the fluxes of particles and the respective energy fluxes are plotted for any frequency smaller than the cutoff ω_{cutoff} , arbitrarily chosen at $\hbar\omega_{\text{cutoff}} \approx 1.3 \text{ eV}$. Note that the range ($\omega_{\text{min}}, \omega_{\text{max}}$) is so narrow to be almost invisible. As a consequence its contribution to the total flux of leftgoing particles is quite small, although the maximum intensity is reached in this range.

Furthermore, the number of particles produced on the

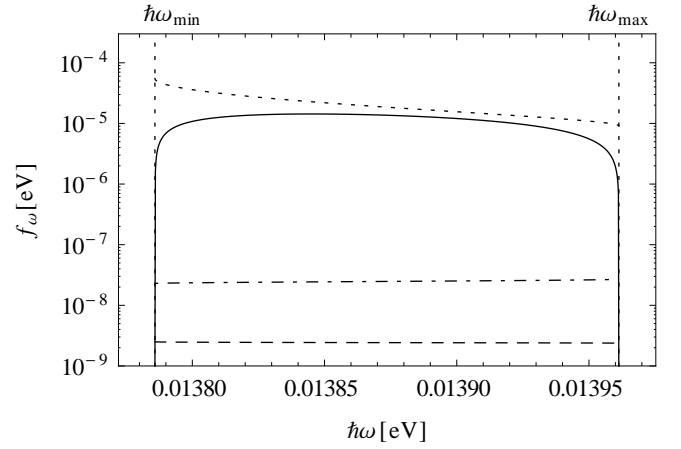


FIG. 8. Energy fluxes f_{ω}^{out} (solid line), $f_{\omega}^{\text{out},l}$ (dashed line), $f_{\omega}^{\text{out},o}$ (dotted line), and $f_{\omega}^{\text{out},u}$ (dot-dashed line), for a configuration with a small refractive index jump ($\delta n \approx 0.001$), obtained with $\epsilon = 0.0026$ [see Eq. (80)]. The pulse velocity has been fine tuned to $v = 0.6838c$, so to have an analogue horizon.

lower and the upper branches are about 3 order of magnitude smaller than the production on the optical branch (both right- and left-going). We have also checked that the main contribution to particle production comes from the incoming negative frequency mode on the optical branch. Both those results confirm that the lower and upper branch can be safely neglected as anticipated in Ref. [20]. Note that the latter result was shown in Fig. 5, for a different configuration with larger refractive index jump.

Finally, in Fig. 10, the energy produced per unit bandwidth and unit time on the rightgoing branch $V_{\omega(\Omega)}^{\text{out}}$ is plotted in the laboratory reference frame. Quite surprisingly the frequency windows is much larger. In fact, even if ω_{min} and ω_{max} almost coincide, k varies in a wider

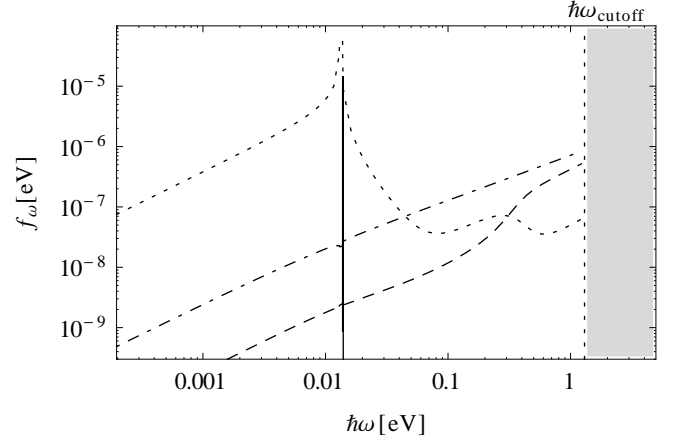
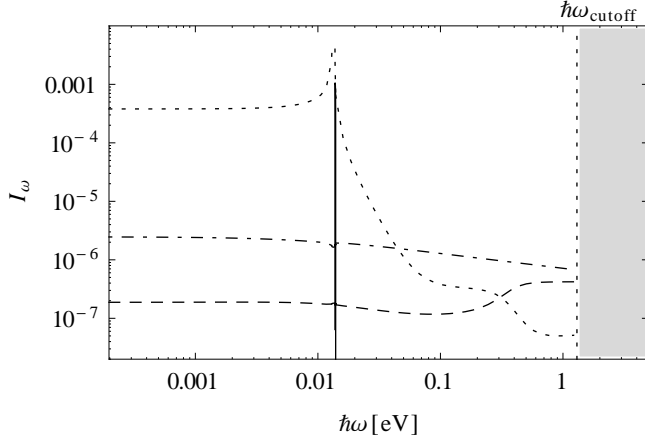


FIG. 9. Fluxes of particles I_{ω}^{out} (solid line), $I_{\omega}^{\text{out},l}$ (dashed line), $I_{\omega}^{\text{out},o}$ (dotted line), $I_{\omega}^{\text{out},u}$ (dot-dashed line) and the respective Energy fluxes f_{ω}^{out} , $f_{\omega}^{\text{out},l}$, $f_{\omega}^{\text{out},o}$, and $f_{\omega}^{\text{out},u}$, for the horizon configuration considered in Fig. 8. The plot has been cutoff at $\omega > \omega_{\text{cutoff}}$. I_{ω}^{out} and f_{ω}^{out} (solid lines) are defined only for $\omega_{\text{min}} < \omega < \omega_{\text{max}}$.

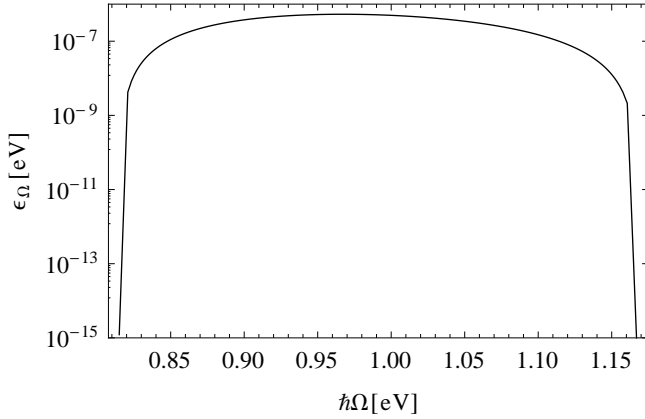


FIG. 10. Energy production rate $\varepsilon_{\Omega}^{\text{out}}$ of the rightgoing mode $V_{\omega(\Omega)}^{\text{out}}$ as seen by an observer in the laboratory, for the horizon configuration considered in Fig. 8.

range, because the group velocity v_g , measured in the comoving frame, almost vanishes. Consequently, from Eq. (28), Ω varies in a quite wide window. However, since the total number of created particles must be the same in both reference frames, the production rate per unit bandwidth is much smaller. Integrating the production rate over frequency and multiplying for $\Delta X_s/V$, with $\Delta X_s \approx 1$ mm, we obtain a tiny average number ($N \approx 8 \times 10^{-4}$) of particles produced by each pulse. In this configuration, fewer particles are produced on the rightgoing mode V_{ω}^{out} , with respect to other modes. In fact, the total number of photons produced on positive norm modes, obtained by integrating all the curves of Fig. 9, left panel, is $N_{\text{tot}} \approx 7 \times 10^{-2}$.

B. Horizonless configuration

A system without any horizon is similar to the case investigated in Sec. IV C for $\omega < \omega_{\text{min}}$ or $\omega > \omega_{\text{max}}$, with the exception that there is now no frequency window with 8 real- k solutions of the dispersion relation in the right region. This configuration can be obtained, as in Ref. [9], by making the pulse so fast that the two rightmost solutions on the optical branch disappear (see Fig. 1, right panel, or Fig. 2, bottom right panel). The pulse velocity is tuned so that the straight dotted line of the bottom panel of Fig. 2 becomes steeper than the tangent to the optical branch at its inflection point.

In analogy with Fig. 1, in Fig. 11 the dispersion relation in the comoving frame is solved only for the optical branch, on both sides of the perturbation, for a pulse with $\delta n = 0.001$ and moving at $v \approx 0.69c$, as in the experiment of Ref. [9]. Only two solutions (one with positive and one with negative norm) are present both in the left ($V_{\omega,L}^o, V_{\omega,L}^{\bar{o}}$) and in the right ($V_{\omega,R}^o, V_{\omega,R}^{\bar{o}}$) regions for all values of the frequency ω . In particular, the solutions corresponding to AMs $V_{\omega,R}^{o2}$ and $V_{\omega,R}$, the mode responsible for analogue Hawking radiation disappear. Even if particle production is still possible, due to the mixing of positive and negative norm frequency modes, the spectrum will be different and the Hawking-like channel is absent. For the sake of completeness, in Fig. 12, the full Sellmeier dispersion relation is graphically solved for this configuration, for $x < 0$ (left panels) and $x > 0$ (right panels).

Finally, the fluxes of emitted photons (Fig. 13) are suppressed by the smallness of δn , as in Sec. V A. The average number of created particles for a pulse which stably propagates for about 1 mm is indeed $N \approx 0.06$. Moreover, the only effect caused by the absence of the horizon is the disappearance of the outgoing rightgoing mode. The integrated (over frequency) number of created particles does not significantly differ with respect to

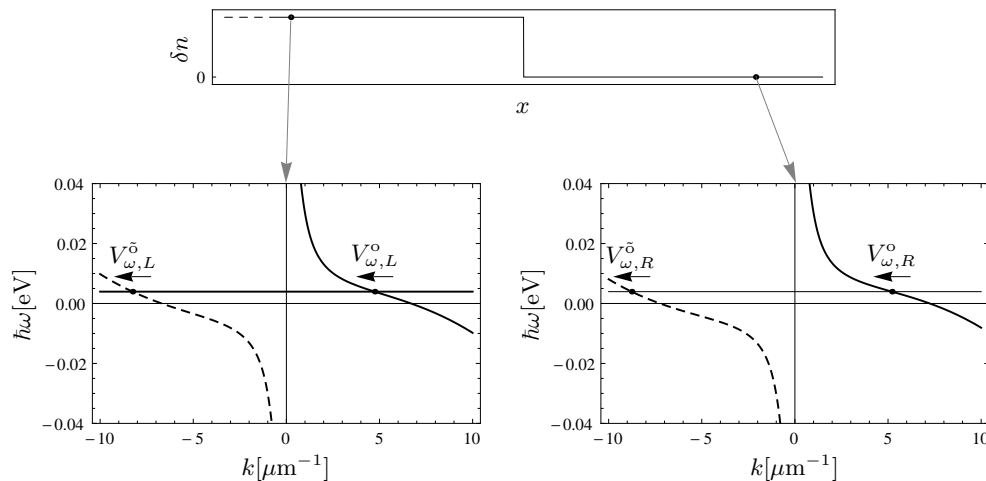


FIG. 11. Simplified analysis of the Sellmeier dispersion relation (27) in fused silica, as seen from the comoving frame. Only the optical branch is shown. Positive (negative) laboratory frequency branches are represented by solid (dashed) curves. The dispersion is plotted on the left ($\delta n = 0.001$, left panel) and on the right of a perturbation ($\delta n = 0$, right panel) moving rightward with $V = 0.69c$ in the laboratory frame (see top panel). For all frequencies there are 2 real solutions both in the left (left panel) and in the right region (right panel). Modes are labeled with the notation introduced in Sec. II and their propagation direction is indicated by arrows.

the horizon configuration with the same small values of δn , because of the narrowness of the frequency window $\omega_{\min} \div \omega_{\max}$.

For the sake of simplicity, the perturbation has been described by a step-like profile. The propagation of light propagating in such optical medium has been modeled by the Lagrangian of the electromagnetic field coupled with polarization fields, in a one-dimensional system.

VI. SUMMARY AND DISCUSSION

In this paper we have developed a microscopic theory of the spontaneous quantum vacuum emission generated by a strong light pulse propagating in a Kerr nonlinear optical medium: the effect of the pulse is modeled as a moving refractive index perturbation following in a local and instantaneous way the pulse. Here we restrict our attention to the case of a single sharp interface separating two homogeneous regions of spatially constant optical properties for which several authors have anticipated the occurrence of the optical analogue of a black hole horizon for suitable values of the pulse speed and the amplitude of the refractive index jump. With respect to previous work, our theory takes into full account the unavoidable frequency refractive index dispersion of the dielectric medium and identifies the different regimes with or without horizon that can be obtained depending on the pulse parameters.

Moving to the reference frame comoving with the pulse where the optical properties of the system are time-independent, the classical eigenmodes of the coupled electromagnetic and matter polarization fields at a given frequency are derived within a Lagrangian formalism and

then quantized through canonical quantization. The mixing of positive and negative norm modes at the same frequency is responsible for the emission of quantum vacuum radiation, whose rate of production has been computed.

In a configuration with horizon, one can identify a quantum vacuum emission channel showing some remarkable similarities with Hawking radiation: this emission channel completely disappears in the absence of horizon and quasi-thermality of its emission spectrum is signaled by an almost constant flux of energy emission when observed in the comoving frame (of course, this spectrum turns out to be distorted when observed in the laboratory frame). On the other hand, because of the nontrivial shape of the Sellmeier dispersion relation, this emission channel is only available and active for frequencies in the restricted $\omega_{\min} < \omega < \omega_{\max}$ range where the analog black hole horizon exists. In addition to this Hawking-like radiation, we have found that quantum vacuum radiation is also emitted on several other channels and outside this frequency window, albeit with a much weaker intensity, a strongly non-thermal spectral distribution, and independently of the presence or not of the horizon. Future work will extend our theory to regimes showing analogue white hole horizons.

As the experiment in [9] was carried out in a parameter range not showing any horizon, it is interesting to conclude the paper by discussing whether or not it is legitimate to denote the quantum vacuum emission in this regime as “Hawking radiation”. This question is all more relevant given the on-going debate [14, 15] on the interpretation of the experimental results. Even if the results of our calculations are objective, answer to this question requires a preliminary agreement on the defini-

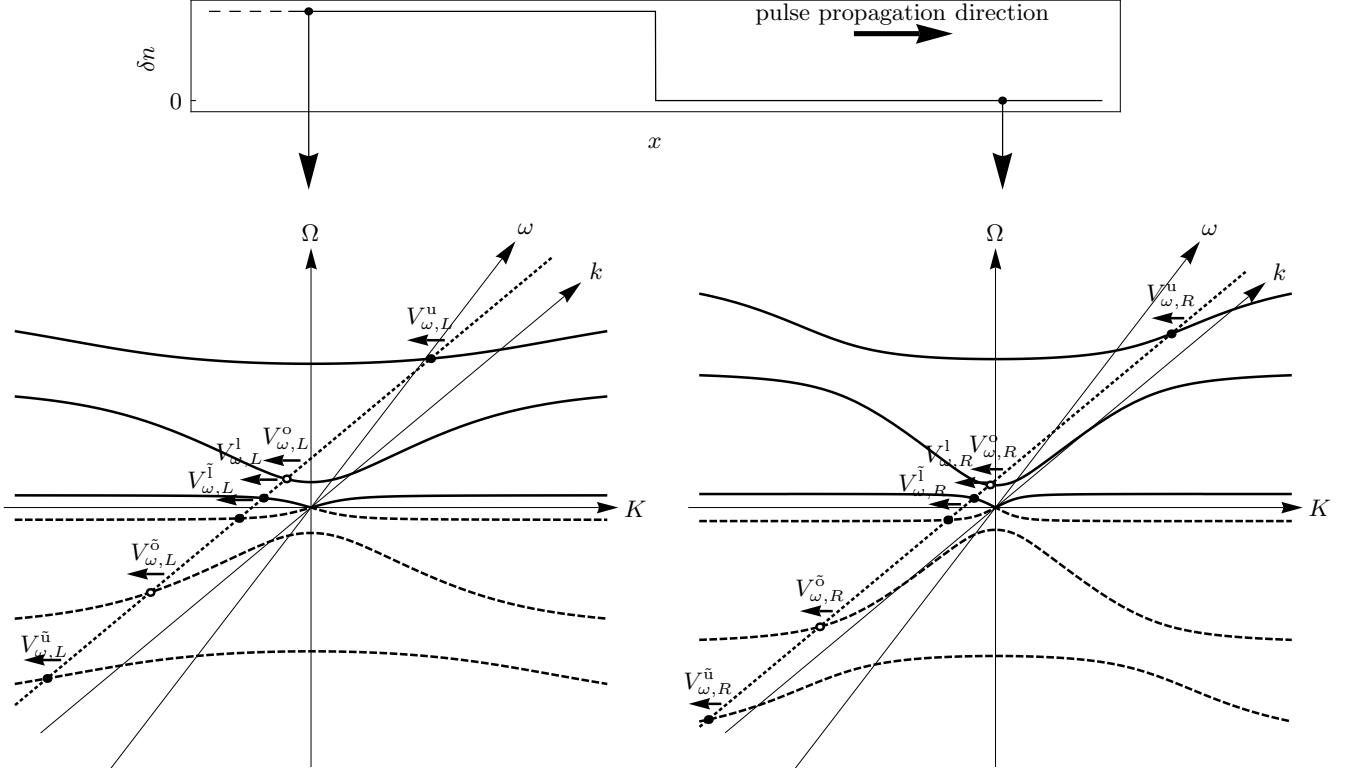


FIG. 12. Graphical representation of the Sellmeier dispersion relation, as seen from the laboratory reference frame (Ω, K) , for $x < 0$ (left panels) and $x > 0$ (right panels). The chosen plot range excludes the highest frequency branch. However, there are no solution on it, see discussion in Sec. III A. The (ω, k) axes of the comoving reference frame are obtained through a boost of velocity v . As sketched in the top panel, the refractive index in the left region is larger than in the right region. This difference in the refractive index is obtained by properly changing the parameters β_i and Ω_i appearing in the Lagrangian (1). In this plot the values of the velocity v and of the refractive index change δn have been arbitrarily chosen for illustrative purposes. The dispersion relation is graphically solved for a fixed comoving frequency ω . Solutions appear both on the positive-norm positive- Ω branches (solid curves) and on the negative-norm negative- Ω branches (dashed curves). The empty dots denote solutions on the optical branches with positive (o) and negative (\bar{o}) frequency Ω . The arrows indicate the direction of propagation (group velocity in the comoving frame) of the associated modes $V_{\omega,L/R}^{\alpha/\bar{\alpha}}$. The dispersion relation has only 6 real- k solutions in both regions.

tion of Hawking radiation, which is somehow a matter of personal taste.

If a broad definition is chosen, where the only requirement is the steady production of particles out of the quantum vacuum, there are no difficulties in considering the predicted emission as an example Hawking radiation. The answer is different if we also require the emission to be thermal, which is definitely not the case of the quantum vacuum emission in horizonless configurations or outside the $\omega_{\min} < \omega < \omega_{\max}$ window of a horizon configurations. And even inside the $\omega_{\min} < \omega < \omega_{\max}$ of a horizon configuration some care has to be paid not to overstretch the gravitational analogy: even if the emission has an approximately thermal spectrum within this window, the fact that it does not extend down to low frequencies is related to the difficulties of a description of the light propagation in terms of a curved space-time metric as done in other analogue models.

VII. ACKNOWLEDGMENTS

We are grateful to D. Faccio for many discussions and explanations about his experiment [9]. We thank R. Balbinot for continuous exchanges and helpful comments about field transformations in a Lagrangian theory, R. Parentani for valuable suggestions about canonical quantization and mode normalizations, S. Liberati and A. Prain for many discussions about the experiment of Ref. [9].

Appendix A: Lagrangian density in the comoving frame

In Sec. II A, we applied a Lorentz boost Λ to the system described by the Lagrangian of Eq. (1), to obtain

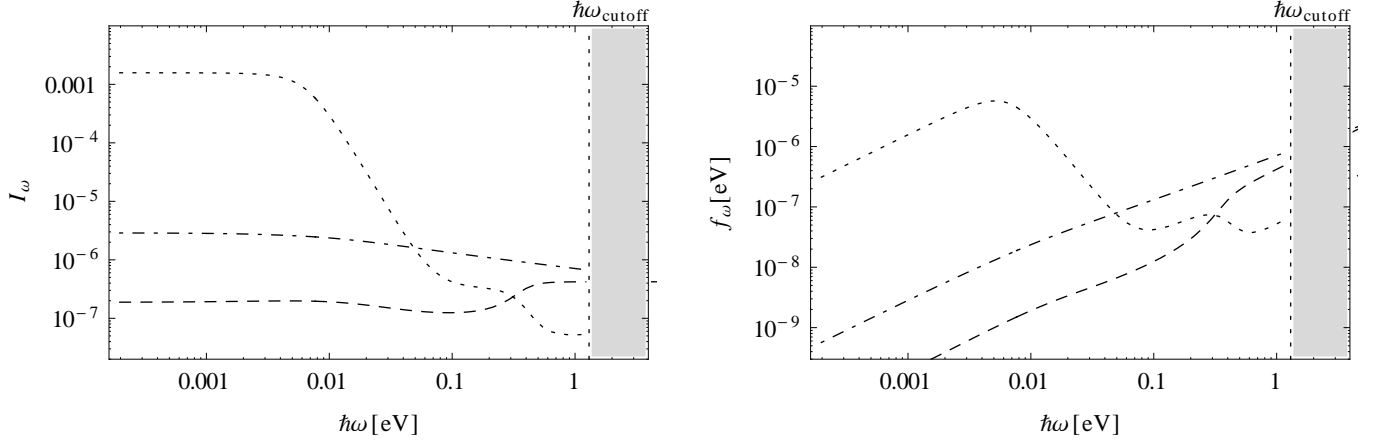


FIG. 13. Occupation numbers $I_{\omega}^{\text{out},l}$ (dashed line), $I_{\omega}^{\text{out},o}$ (dotted line), $I_{\omega}^{\text{out},u}$ (dot-dashed line) and the corresponding energy fluxes (right panel) f_{ω}^{out} , $f_{\omega}^{\text{out},l}$, $f_{\omega}^{\text{out},o}$, and $f_{\omega}^{\text{out},u}$, for a horizonless configuration. The velocity of the pulse and the variation of the refractive index are chosen to reproduce the experimental configuration of Ref. [9]: $v = 0.69c$ and $\epsilon = 0.0026$, yielding via Eq. (80) a jump in the refractive index of $\delta n = 0.001$.

Eq. (4). In doing so, we transformed the space and time coordinates, but we treated both the fields A and P as scalars.¹ This is possible since we are dealing with a 1+1 dimensional system.

To properly proceed, one should first apply the Lorentz transformation Λ to the fields A and P , assuming that both A and P oscillate in the z direction. A is the z component of the electromagnetic potential

$$A^{\mu} = \begin{pmatrix} 0 \\ 0 \\ 0 \\ A \end{pmatrix}, \quad (\text{A1})$$

which transform as

$$A_p^{\mu} = \Lambda^{\mu}_{\nu} A^{\nu}, \quad (\text{A2})$$

where the subscript p indicates that A_p^{μ} is measured in the reference frame comoving with the pulse. Analogously, P is one of the three components of the magnetization-polarization tensor

$$M^{\mu\nu} = \begin{pmatrix} 0 & cP_x & cP_y & cP_z \\ -cP_x & 0 & -M_z & M_y \\ -cP_y & M_z & 0 & -M_x \\ -cP_z & -M_y & M_x & 0 \end{pmatrix} = \begin{pmatrix} 0 & 0 & 0 & cP \\ 0 & 0 & 0 & 0 \\ 0 & 0 & 0 & 0 \\ -cP & 0 & 0 & 0 \end{pmatrix}, \quad (\text{A3})$$

which transform as

$$M_p^{\mu\nu} = \Lambda^{\mu}_{\rho} \Lambda^{\nu}_{\sigma} M^{\rho\sigma}. \quad (\text{A4})$$

By doing so, the Lagrangian density can be rewritten in term of the new fields A_p^{μ} and $M_p^{\mu\nu}$.

Moreover, the Lagrangian density can always be expressed by using new fields that are functions of A_p^{μ} and $M_p^{\mu\nu}$, provided that the transformation to those new fields does not involve any time derivative of A_p^{μ} and $M_p^{\mu\nu}$. Such a transformation generates a canonical transformation on the Hamiltonian variables, so that the commutation rules among the new fields and their respective momenta are still canonical. We chose to apply to A_p^{μ} and $M_p^{\mu\nu}$ the linear transformation Λ^{-1} , not involving any time derivative of the fields. The new fields A_n^{μ} and $M_n^{\mu\nu}$ are

$$\begin{aligned} A_n^{\mu} &\equiv (\Lambda^{-1})^{\mu}_{\nu} A_p^{\nu} = (\Lambda^{-1})^{\mu}_{\nu} \Lambda^{\nu}_{\rho} A^{\rho} = A^{\mu} \\ M_n^{\mu\nu} &\equiv (\Lambda^{-1})^{\mu}_{\rho} (\Lambda^{-1})^{\nu}_{\sigma} M_p^{\rho\sigma} \\ &= (\Lambda^{-1})^{\mu}_{\rho} (\Lambda^{-1})^{\nu}_{\sigma} \Lambda^{\rho}_{\alpha} \Lambda^{\sigma}_{\beta} M_p^{\alpha\beta} = M^{\mu\nu}. \end{aligned} \quad (\text{A5})$$

That is, A_n^{μ} and $M_n^{\mu\nu}$ coincide with the old fields A^{μ} and $M^{\mu\nu}$, as measured in the laboratory frame. The only nonvanishing components of those fields are A and P , as in Eqs. (A1) and (A3).

Appendix B: Mode normalization

The scalar product (18) on two eigenmodes with real frequencies ω_1 and ω_2 , and real momenta k_{α_1} and k_{α_2} is

$$\begin{aligned} \langle V_{\omega_1}^{\alpha_1}, V_{\omega_2}^{\alpha_2} \rangle &= \frac{i}{\hbar} \int dx e^{-i(\omega_2 - \omega_1)t + i(k_{\alpha_2} - k_{\alpha_1})x} \bar{V}_{\omega_1}^{\alpha_1 \dagger} \eta \bar{V}_{\omega_2}^{\alpha_2} \\ &= 2\pi \delta(k_{\alpha_2} - k_{\alpha_1}) e^{-i(\omega_2 - \omega_1)t} \bar{V}_{\omega_1}^{\alpha_1 \dagger} \eta \bar{V}_{\omega_2}^{\alpha_2}. \end{aligned} \quad (\text{B1})$$

This proves that modes with different momenta are orthogonal. However, for each value of k there are 8 solutions ω of the dispersion relation (27). Thus, there are modes with different frequencies $\omega_1 \neq \omega_2$ which share the same momentum $k_{\alpha_1} = k_{\alpha_2}$. We shall show that modes with different frequencies ω_1 and ω_2 are also orthogonal.

¹ To maintain the notation compact, the subscript i is omitted in this Appendix.

We start from the identity

$$\bar{V}_{\omega_1}^{\alpha_1 \dagger} \eta [i\eta \mathcal{K}(k) - i\eta \mathcal{K}(k)] \bar{V}_{\omega_2}^{\alpha_2} = 0, \quad (\text{B2})$$

computed for two modes with the same momentum $k_{\alpha_1} = k_{\alpha_2} = k$. Using the relations $\eta^2 = -I_8$, $\eta^\dagger \eta = I_8$, and $\mathcal{K}^\dagger = \mathcal{K}$:

$$(i\eta \mathcal{K} \bar{V}_{\omega_1}^{\alpha_1})^\dagger \eta \bar{V}_{\omega_2}^{\alpha_2} - \bar{V}_{\omega_1}^{\alpha_1 \dagger} \eta (i\eta \mathcal{K} \bar{V}_{\omega_2}^{\alpha_2}) = 0. \quad (\text{B3})$$

Since both modes are solutions of Eq. (23), we obtain

$$(\omega_1 - \omega_2) \bar{V}_{\omega_1}^{\alpha_1 \dagger} \eta \bar{V}_{\omega_2}^{\alpha_2} = 0, \quad (\text{B4})$$

which shows that $\bar{V}_{\omega_1}^{\alpha_1 \dagger} \eta \bar{V}_{\omega_2}^{\alpha_2}$ vanishes if $\omega_1 \neq \omega_2$. Since, at fixed k ω can take only a finite set of values, it is possible to write

$$\bar{V}_{\omega_1}^{\alpha_1 \dagger} \eta \bar{V}_{\omega_2}^{\alpha_2} = \delta_{\omega_2 \omega_1} \bar{V}_{\omega_2}^{\alpha_1 \dagger} \eta \bar{V}_{\omega_2}^{\alpha_2}. \quad (\text{B5})$$

Putting this expression in Eq. (B1)

$$\langle V_{\omega_1}^{\alpha_1}, V_{\omega_2}^{\alpha_2} \rangle = 2\pi \delta(k_{\alpha_2} - k_{\alpha_1}) \delta_{\omega_2 \omega_1} \frac{i}{\hbar} \bar{V}_{\omega_2}^{\alpha_1 \dagger} \eta \bar{V}_{\omega_2}^{\alpha_2} \quad (\text{B6})$$

and noting that

$$\delta(k_{\alpha_2} - k_{\alpha_1}) \delta_{\omega_2 \omega_1} = \left| \frac{d\omega}{dk} \right|_{k=k_{\alpha_2}} \delta(\omega_2 - \omega_1) \delta_{k_{\alpha_2} k_{\alpha_1}}, \quad (\text{B7})$$

the combination of Dirac and Kroenecker δ 's appearing in Eq. (B6) can be rewritten as

$$\left| \frac{d\omega}{dk} \right|_{k=k_{\alpha_2}} \delta(\omega_2 - \omega_1) \delta_{\alpha_2 \alpha_1}, \quad (\text{B8})$$

where, as said, α labels the 8 solutions with different momentum, sharing the same comoving frequency ω .

In conclusion, we proved that eigenmodes with different ω and k_α are orthogonal:

$$\langle V_{\omega_1}^{\alpha_1}, V_{\omega_2}^{\alpha_2} \rangle = 2\pi \left| \frac{d\omega}{dk} \right|_{k=k_{\alpha_2}} \delta(\omega_2 - \omega_1) \delta_{\alpha_2 \alpha_1} \frac{i}{\hbar} \bar{V}_{\omega_2}^{\alpha_2 \dagger} \eta \bar{V}_{\omega_2}^{\alpha_2}, \quad (\text{B9})$$

where the last term of this expression is easily computed from Eq. (30):

$$i \bar{V}_{\omega}^{\alpha \dagger} \eta \bar{V}_{\omega}^{\alpha} = \frac{|C_{\omega}^{\alpha}|^2}{2\pi} \left[\omega + \sum_{i=1}^3 \frac{4\pi\beta_i \gamma^2 (\omega + vk)}{[1 - \gamma^2 (\omega + vk)^2 / \Omega_i^2]^2} \right], \quad (\text{B10})$$

where, for the sake of conciseness, the index α is omitted on the right hand side. By using the Lorentz transformation (28):

$$i \bar{V}_{\omega}^{\alpha \dagger} \eta \bar{V}_{\omega}^{\alpha} = \frac{\gamma |C_{\omega}^{\alpha}|^2}{2\pi} \left\{ -vK + \Omega \left[1 + \sum_{i=1}^3 \frac{4\pi\beta_i}{(1 - \Omega^2 / \Omega_i^2)^2} \right] \right\}. \quad (\text{B11})$$

Note that the scalar product is not positive definite. Thus, we must characterize under what conditions a mode has indeed positive or negative norm.

From the dispersion relation in the glass rest frame (29), the group velocity V_g in the laboratory frame is given by

$$V_g^{-1} = \frac{dK}{d\Omega} = \frac{\Omega}{K} \frac{dK^2}{d\Omega^2} = \frac{\Omega}{c^2 K} \left[1 + \sum_{i=1}^3 \frac{4\pi\beta_i}{(1 - \Omega^2 / \Omega_i^2)^2} \right], \quad (\text{B12})$$

so that

$$i \bar{V}_{\omega}^{\alpha \dagger} \eta \bar{V}_{\omega}^{\alpha} = \frac{\gamma c^2 |C_{\omega}^{\alpha}|^2}{2\pi} \frac{K}{V_g} \left(1 - \frac{vV_g}{c^2} \right). \quad (\text{B13})$$

Since there is no absorption, the group velocity $|V_g|$ must be smaller than the speed of light c [32]. Furthermore $v < c$, so that the parenthesis in Eq. (B13) is always positive. Furthermore, the sign of V_g is positive (negative) if Ω and K have the same (opposite) sign [see Eq. (B12)]. As a consequence, the sign of the above scalar product is always equal to the sign of Ω , i.e., modes with positive (negative) rest frame frequency Ω have positive (negative) norm.

Finally, the normalization constant C_{ω}^{α} , appearing in Eq. (30) is fixed by imposing

$$|\langle V_{\omega_1}^{\alpha_1}, V_{\omega_2}^{\alpha_2} \rangle| = \delta(\omega_2 - \omega_1) \delta_{\alpha_2 \alpha_1}, \quad (\text{B14})$$

for both positive and negative norm modes, and by comparing the above condition with Eqs. (B9) and (B13):

$$|C_{\omega}^{\alpha}|^2 = \left| \frac{\gamma c^2}{\hbar} \frac{v_g}{V_g} \left(1 - \frac{vV_g}{c^2} \right) K \right|^{-1}. \quad (\text{B15})$$

Using the relativistic composition of velocities

$$v_g = \frac{V_g - v}{1 - vV_g/c^2}, \quad (\text{B16})$$

Eq. (B13) simplifies to

$$|C_{\omega}^{\alpha}|^2 = \left| \frac{\gamma c^2}{\hbar} \left(1 - \frac{v}{V_g} \right) K \right|^{-1}. \quad (\text{B17})$$

Replacing V_g from Eq. (B12)

$$|C_{\omega}^{\alpha}|^2 = \hbar \left| c^2 \gamma \left(K - \frac{v}{c^2} \Omega \right) - v \sum_{i=1}^3 \frac{4\pi\beta_i \gamma \Omega_i}{(1 - \Omega^2 / \Omega_i^2)^2} \right|^{-1}, \quad (\text{B18})$$

and going back to the comoving frame frequency ω and momentum k_{α} :

$$|C_{\omega}^{\alpha}|^2 = \hbar \left| c^2 k_{\alpha} - v \sum_{i=1}^3 \frac{4\pi\beta_i \gamma^2 (\omega - vk_{\alpha})}{[1 - \gamma^2 (\omega - vk_{\alpha})^2 / \Omega_i^2]^2} \right|^{-1}. \quad (\text{B19})$$

-
- [1] S. W. Hawking, *Nature* **248**, 30 (1974)
 - [2] S. W. Hawking, *Commun. Math. Phys.* **43**, 199 (1975)
 - [3] W. G. Unruh, *Phys. Rev. Lett.* **46**, 1351 (1981)
 - [4] C. Barcelo, S. Liberati, and M. Visser, *Living Rev. Rel.* **14**, 3 (2011)
 - [5] T. G. Philbin, C. Kuklewicz, S. Robertson, S. Hill, F. König, and U. Leonhardt, *Science* **319**, 1367 (2008)
 - [6] U. Leonhardt and T. G. Philbin (Elsevier, 2009) pp. 69–152
 - [7] D. Gerace and I. Carusotto (2012), [arXiv:1206.4276 \[cond-mat.quant-gas\]](#)
 - [8] M. Elazar, V. Fleurov, and S. Bar-Ad, ArXiv e-prints (Jun. 2012), [arXiv:1206.5964 \[physics.optics\]](#)
 - [9] F. Belgiorno, S. L. Cacciatori, M. Clerici, V. Gorini, G. Ortenzi, L. Rizzi, E. Rubino, V. G. Sala, and D. Faccio, *Phys. Rev. Lett.* **105**, 203901 (2010)
 - [10] E. Rubino, F. Belgiorno, S. L. Cacciatori, M. Clerici, V. Gorini, G. Ortenzi, L. Rizzi, V. G. Sala, M. Kolesik, and D. Faccio, *New J. Phys.* **13**, 085005 (2011)
 - [11] J. Durnin, J. J. Miceli, Jr., and J. H. Eberly, *Phys. Rev. Lett.* **58**, 1499 (1987)
 - [12] F. Gori, G. Guattari, and C. Padovani, *Opt. Commun.* **64**, 491 (1987)
 - [13] K. T. McDonald [arXiv:physics/0006046](#)
 - [14] R. Schützhold and W. G. Unruh, *Phys. Rev. Lett.* **107**, 149401 (2011)
 - [15] F. Belgiorno, S. L. Cacciatori, M. Clerici, V. Gorini, G. Ortenzi, L. Rizzi, E. Rubino, V. G. Sala, and D. Faccio, *Phys. Rev. Lett.* **107**, 149402 (2011)
 - [16] S. Liberati, A. Prain, and M. Visser, *Phys. Rev. D* **85**, 084014 (2012)
 - [17] W. G. Unruh and R. Schützhold [arXiv:1202.6492 \[quant-ph\]](#)
 - [18] S. J. Robertson, “Hawking Radiation in Dispersive Media,” (2011), [arXiv:1106.1805 \[gr-qc\]](#)
 - [19] U. Leonhardt and S. Robertson, *New J. Phys.* **14**, 053003 (2012)
 - [20] S. Finazzi and I. Carusotto [arXiv:1204.3603 \[physics.optics\]](#)
 - [21] P. Butcher and D. Cotter, *The Elements of Nonlinear Optics* (Cambridge University Press, Cambridge, 1991)
 - [22] J. J. Hopfield, *Phys. Rev.* **112**, 1555 (1958)
 - [23] I. Carusotto, M. Antezza, F. Bariani, S. de Liberato, and C. Ciuti, *Phys. Rev. A* **77**, 063621 (2008)
 - [24] C. Ciuti, G. Bastard, and I. Carusotto, *Phys. Rev. B* **72**, 115303 (2005)
 - [25] I. Carusotto, S. de Liberato, D. Gerace, and C. Ciuti, *Phys. Rev. A* **85**, 023805 (2012)
 - [26] Sellmeier, *Annalen der Physik* **219**, 272 (1871)
 - [27] “Refractive index database, <http://refractiveindex.info>,”
 - [28] S. Finazzi and R. Parentani, *Phys. Rev. D* **85**, 124027 (2012)
 - [29] J. Macher and R. Parentani, *Phys. Rev. D* **79**, 124008 (2009)
 - [30] A. Recati, N. Pavloff, and I. Carusotto, *Phys. Rev. A* **80**, 043603 (2009)
 - [31] J. Macher and R. Parentani, *Phys. Rev. A* **80**, 043601 (Oct. 2009)
 - [32] L. Landau, E. Lifshitz, and L. Pitaevskii, *Electrodynamics of continuous media*, Course of theoretical physics (Butterworth-Heinemann, 1984)